Bioactive Materials 5 (2020) 902–916

Contents lists available at ScienceDirect

Bioactive Materials

journal homepage: http://www.keaipublishing.com/biomat

Microbial ingress and *in vitro* degradation enhanced by glucose on bioabsorbable Mg–Li–Ca alloy

Ling-Yu Li[a], Zhuang-Zhuang Han[a], Rong-Chang Zeng[a,d,*], Wei-Chen Qi[a], Xiao-Fan Zhai[b], Yi Yang[c], Yun-Tian Lou[c], Tingyue Gu[e], Dake Xu[c,**], Ji-Zhou Duan[b,***]

[a] Corrosion Laboratory for Light Metals, College of Material Science and Engineering, Shandong University of Science and Technology, Qingdao, 266590, China
[b] Institute of Oceanology, Chinese Academy of Sciences, Qingdao, 266590, China
[c] Shenyang National Laboratory for Materials Science, Northeastern University, Shenyang, 110819, China
[d] School of Materials Science and Engineering, Zhengzhou University, Zhengzhou, 450002, China
[e] Department of Chemical & Biomolecular Engineering, Russ College of Engineering and Technology, Ohio University, Athens, OH, 45701-2979, USA

ARTICLE INFO

Keywords:
Glucose
Magnesium
Bacteria
Biomaterial
Biodegradation

ABSTRACT

Biodegradable magnesium alloys are challenging to be implanted in patients with hyperglycemia and diabetes. A hypothesis is suggested that glucose accelerates microbial ingress and *in vitro* degradation of Mg–Li–Ca implants. Corrosion resistance and mechanical properties was demonstrated using electrochemical, hydrogen evolution and tensile tests. The bacteria from Hank's solution were isolated via 16S rRNA gene analysis. The results revealed that Mg–1Li–1Ca alloy exhibited different responses to Hank's solution with and without glucose. The solution acidity was ascribed to Microbacterium hominis and Enterobacter xiangfangensis, indicating that glucose promoted microbial activity and degradation and deterioration in mechanical property of Mg–1Li–1Ca alloy.

1. Introduction

For a number of years, major public health concerns have been raised regarding the hazards posed by population ageing, especially the prevalence of hyperglycemia (high blood glucose) and diabetes [1–3]. There are several critical issues to be considered in accessing these hazards, including obesity, poor diet, and physical inactivity, as well as a host of negative health problems that associated with osteoporosis, heart disease, stroke, neuropathy, and kidney disease [4–6]. Moreover, the presence of diabetic foot implies the relationship of inflection with high content glucose [7]. Thereby, the global trend of aging population increases the demand for biomaterials, which have to face enormous challenge to be implanted in the patients with hyperglycemia and diabetes.

Artificial biomaterials include metals, polymers and ceramics and their composites [8,9]. Particularly, inert metals, such as stainless steels and titanium alloys [10], have high mechanical strength and corrosion resistance, which are predominately used as orthopedic implants. However, magnesium (Mg) and its alloys with a density below 2 g/cm^3 are biodegradable and have a close elastic modulus to bone [11]. Thus, Mg and its alloys as next generation biodegradable metallic implant have been extensively investigated in recent decades [12–15], especially with their unique ability to proliferate the differentiation and growth of human osteoblasts [16–18]. Mg is the 4th most abundant cation in human body. The total body contains 21–28 g Mg for an average 70-kg adult. Mg deficiency has been involved in the diseases of diabetes, hypertension and so on.

In our previous study, we systematic investigated *in vitro* degradation of pure Mg in response to glucose [3]. Our finding indicated that the degradation rate of pure Mg was decreased with increasing glucose content in Hank's solution due to transformation of glucose into gluconic acid, which gluconic acid can coordinates Ca^{2+} ions in Hank's solution and thus form Ca–P layer on the sample surface. Furthermore, high glucose concentration lower degradation and pH value more.

On the other hand, the introduction of an implant in the body is always connected with the risk of bacterial infection, particularly for

Peer review under responsibility of KeAi Communications Co., Ltd.
* Corresponding author. Corrosion Laboratory for Light Metals, College of Material Science and Engineering, Shandong University of Science and Technology, Qingdao, 266590, China.
** Corresponding author.
*** Corresponding author.
E-mail addresses: rczeng@foxmail.com (R.-C. Zeng), xudake@mail.neu.edu.cn (D. Xu), duanjz@qdio.ac.cn (J.-Z. Duan).

https://doi.org/10.1016/j.bioactmat.2020.06.014
Received 31 March 2020; Received in revised form 7 June 2020; Accepted 8 June 2020

the fixation of open-fractured bones and joint-revision surgeries [19,20]. Bacterial infections represent significant hurdles in the management of both surgical and traumatic wounds and contribute considerably to increased morbidity and mortality, regardless of the source or location. The significance of this problem is underscored when one considers that orthopedic implant-related infections occur in nearly 112,000 human patients annually and create a $2 billion burden for the US healthcare industry [21]. Early implant failure is commonly associated with certain strains of bacteria. The most common bacteria, involved in these types of infections, include: streptococci, anaerobic Gram positive cocci, and anaerobic gram negative rods [22]. Therefore, bacterial-induced corrosion or degradation of the implanted metals becomes a major concern.

Magnesium is the molecular key that can activate many important enzymes responsible for various biochemical reactions in living cells, which is regarded as one of the intracellular bulk elements and involved in enzyme catalysis [23–25]. Moreover, Mg is one of the major cell components of bacteria, which predispose the Mg surface to microbial attachment and growth [26]. Unfortunately, few studies have focused on the significant influence of microbial ingress to biodegradation of Mg alloys *in vitro*. Zhu et al. [27] suggested that sulfate-reducing bacteria (SRB), a kind of anaerobic bacteria predominantly living in soil and water, play an important part in the corrosion process of the AZ91D Mg alloy. In presence of SRB, pitting corrosion occurs on the sample surface, leading to a change in stress distribution and stress concentration. As a result, SRB promotes the severe drop in the residual strength by corrosion induced microbiological activity. As the first basic step to investigate the degradation behavior of biomaterials, *in vitro* experiment should be carried out in simulated body fluids (SBF), i.e. Hank's solution, in order to save time and reduce cost. Normally, the *in vitro* corrosion evaluation of biomedical Mg alloys has been performed in laboratory without any sterilization treatment in open air. Hence, it is possible for all kinds of bacteria to adhere and grow on Mg alloys that leads to microbiologically influenced corrosion (MIC), especially for a longer immersion without any solution refreshing.

Generally, the MIC of Mg alloys is often ignored due to anti-bacterial function of Mg ions and alkaline environment during the degradation of Mg alloys in immersion test. On the cases of MIC, bacterial biofilm may form on Mg surface and can be a possible threat to Mg deterioration [28]. Moreover, the acidic metabolite of bacteria may neutralize the basic corrosion products of the Mg substrate in the immersion medium. In this work, we set out to systematically assay interaction between Mg alloys and microorganism measuring the condition of Mg surface, and identifying bacteria community or colony in Hank's solution. On the other hand. To better understand the roles of glucose, as the major organic carbon source affecting bacterial activity, we characterized systemic experiments on the growth and classification of lab bacteria via 16S rRNA gene analysis, degradation behavior and mechanical performance of the alloy using glucose-free solution to elucidate the microbial degradation mechanism. In addition, attempts to reduce bacterial activity was also conducted.

2. Methods

Sample preparation. The ingots of Mg–1Li–1Ca alloy with chemical compositions of 0.88 wt% Li, 1.12 wt % Ca, and balanced Mg were fabricated at the institute of Metals Research, the Chinese Academy of Sciences. The ingots were then extruded into sheets on an extrusion machine at an extrusion ratio of 15.7:1 and an extrusion rate of 22 mm/s. The mould and the ingots were heated up to the temperature of 430 °C and 400 °C, respectively.

Immersion tests. The Mg specimen was put in a beaker with Hank's solution. A funnel with scale was placed over the specimen, on which a polytetrafluoroethylene (PTFE) plate with Φ 20 mm through-holes was placed to ensure the collection of hydrogen and the back of the specimen exposed to the Hank's solution, which contains 8.0 g/L NaCl, 0.4 g/L KCl, 0.14 g/L $CaCl_2$, 0.35 g/L $NaHCO_3$, 1.0 g/L glucose ($C_6H_6O_6$), 0.1 g/L $MgCl_2{\cdot}6H_2O$, 0.06 g/L $MgSO_4{\cdot}7H_2O$, 0.06 g/L KH_2PO_4 and 0.06 g/L $Na_2HPO_4{\cdot}12H_2O$ at 37 ± 0.5 °C. A burette was mounted over the funnel and filled with the test solution. The volume of evolved hydrogen and solution pH value was simultaneously able to be measured per hour in the setup. The ratio of the specimen area to the solution volume was maintained at 45 mL/cm^2. The pH values of the solutions were recorded by a pH meter (pH400 type).

Surface analysis. The electron probe X-ray microanalysis (EPMA, JXA-8230) was used to analyze the morphology and EDS of the corrosion product layer on the alloy surface. Also, the constituent of corrosion products was examined by means of X-ray diffraction (XRD, D/Max2500PC) and Fourier transformed infrared (FTIR, Nicolet 380).

Fluorescence microscopy observation. The Mg–1Li–1Ca alloy immersed in Hank's solution in specific time (1 h, 6 h, 24 h, 48 h, 96 h, and 144 h). Samples dried with cool air stream after immersion, sterilized with 5% glutaraldehyde for 1 h. Then these specimens washed with a sterile phosphate buffered saline (PBS) solution to remove the loosely attached bacteria, stained in the dark for 15 min with 0.1% DAPI, then observed the bacteria with Olympus BX51 fluorescence microscope.

Tensile test. Tensile sample machined by wire-electrode cutting were polished with silicon carbide papers from 150 grit to 1500 grit. The tensile tests were performed at a strain rate of 10^{-3}/s under ambient temperature on an electronic universal testing machine (WDW-100). Each measurement was carried out in triplicate.

Bacteria isolate. Using Luria-Bertani (LB), Tryptic Soy Agar (TSA), Potato Dextrose Agar (PDA) and De Mann, Rogosa and Sharpe (MRS) five kinds medium to isolate bacteria. The magnesium coupons were immersed into the Hank's solution. After 2 days, the pH value of the solution became decrease. Spread 100 μL acidy Hank's solution on these five kinds medium plates. Place the plates in 37 °C incubator overnight. Then, streaking the plates to isolate individual colonies. Incubate the individual colonies on the agar plate to receive the pure strains. Dissolve the pure strains to 1 mL (about 1–2 × $10^{\hat{}9}$ CFU/mL) bacteria suspension. The suspension was processed for DNA extraction using the TAKARA Bacterial Genomic DNA Extraction Kit Ver.3.0 according to manufacturer's protocols. Polymerase chain reaction (PCR) amplification of bacterial DNA. Then, using the *16S rRNA* method to identify the bacteria.

Bacterial influenced immersion tests. Culturing the isolated bacteria of Microbacterium hominis and Enterobacter xiangfangensis and using saline solution to dilute around 10^9 CFU/mL. Then adding 1 mL bacterial suspensions to sterilized Hank's solution, respectively. All Mg–1Li–1Ca alloy samples were placed under UV irradiation for 30 min. Herein, the detailed immersion tests were similar to previous immersion tests.

3. Results

3.1. Influence of glucose in Hank's solution on pH and HER

Hydrogen evolution rate (HER) and pH values of Mg–1Li–1Ca exposed to Hank's solution at 37 ± 0.5 °C for 168 h are displayed in Fig. 1a. The change in HERs experienced three stages: it was lower at the initial immersion of 30 h, and subsequently climbed up during the immersion of 42 h, and then dripped slowly with extending immersion time. Interestingly, pH value of the solution has an initial increase during the first 3 h that corresponding to the conventional corrosion of Mg alloy. Generally, Mg is very active in Hank's solution. Once immersed in solution, the sample of Mg would dissolve and release a vast number of Mg^{2+} ions (reaction 1), alkaline hydroxyl anions and H_2 gas (reaction 2), resulting in a quick rise in pH value. However, the pH value of the solution sharply decreased to 5.0 in the next around 72 h, and then rebounded due to the severe corrosion occurred gave rise to a rise in pH value. This scenario is tremendously different from the

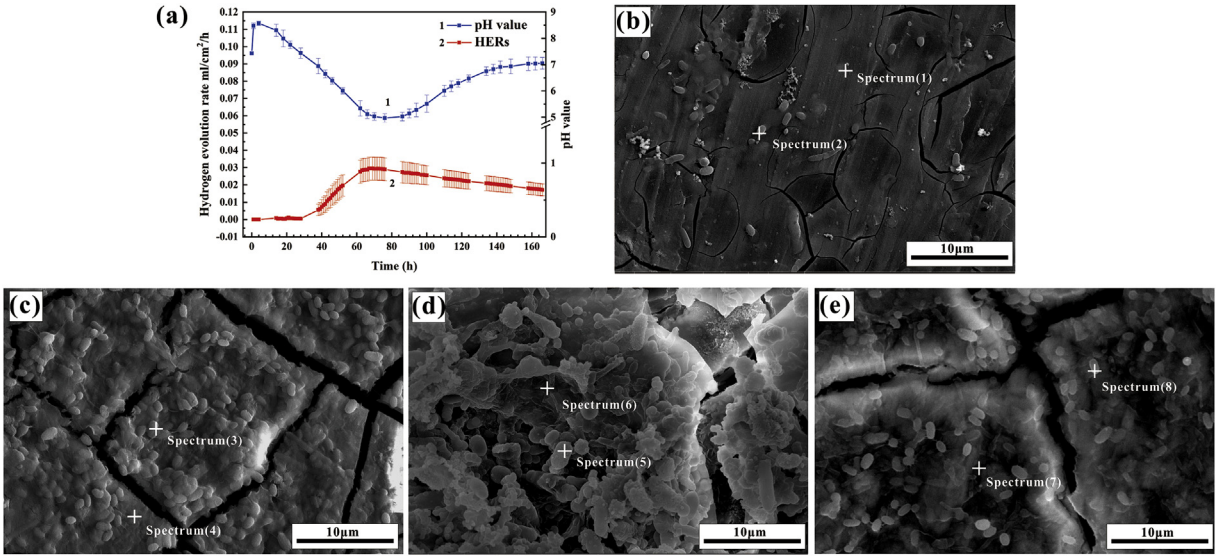

Fig. 1. (a) Hydrogen evolution rate (HER) and pH values of Mg–1Li–1Ca samples immersed in presence of 1.0 g/L glucose in Hank's solution for 168 h at 37 ± 0.5 °C; SEM morphologies of Mg–1Li–1Ca after immersion in Hank's solution for different time: (b) 24 h, (c) 48 h, (d) 96 h, and (e) 168 h.

conventional immersion test of Mg alloys [29]. Therefore, a further exploration was necessary to make sure the degradation mechanism.

$$Mg\ (s) \rightarrow Mg^{2+}(aq) + 2e^{-} \quad [1]$$

$$2H_2O\ (aq) + 2e^{-} \rightarrow 2OH^{-}(aq) + H_2\uparrow \quad [2]$$

To present the surface situation of the substrate during immersion test, a series of SEM images at specific time (24 h, 48 h, 96 h and 168 h) have been illustrated in Fig. 1 b-e and the energy dispersive spectroscopy (EDS) results of specific spectrum have been showed in spectrum (1)–(8). All samples were subjected to corrosion with cracks at different levels. As shown in Fig. 1b, a small amount of rod-like precipitates formed on the sample surface. With time extended to 48 h (Fig. 1c), numerous rod-like particles deposited on the entire surface with deep and wide cracks, forming incomplete biofilm on Mg substrate. When immersion time was prolonged to 96 h (Fig. 1d), irregular product covered on the surface along with biofilm collapsed. After soaking for 168 h (Fig. 1e), the amount of rod-like particulates declined on the substrate.

The EDS results (Table 1) are conduced to confirm the species (i.e. bacteria) in Fig. 1b–e. The primary elements formed on Mg–1Li–1Ca surface after immersion in different time are quite diverse. The predominant components of Spectrum #1 and 2 were Mg, O and C, in addition to trace amounts of Ca and P that mainly came from corrosion products. However, after 48 h of immersion, Spectrum #3 exhibits high percent of C, N and trace of S. C demonstrates the presence of carboxyl (-COOH) groups in gluconic acid from the transformation of glucose [3], amino acids and other species (C–N etc.); N designates the presence of amino (-NH_2) group of amino acids; whereas S only existed in two amino acids: cysteine and methionine [30,31], indicating that a large amount of bacteria colonies were attached to the sample surface. Spectrum #4 has the similarly composition with Spectrum #3, but displays higher percent of S element and none N element, which implies that the bacteria colonies inhomogeneous covered on the sample surface. It is also near in this stage HERs were remarkably increased and pH values were sharply decreased due to enhanced bacterial metabolic activity. After immersion for 96 h (Spectrum #5 and 6), the Ca and P contents considerately improved, implying that more Ca–P compounds were deposited on the sample surface, which were in accordance with SEM results that more rod-like bacteria colonies appeared and became

Table 1
EDS analysis data of Mg–1Li–1Ca alloy immersed in Hank's solution in Fig. 1 in wt.% (at. %).

Elements	Spectrum							
	#1	#2	#3	#4	#5	#6	#7	#8
Mg	85.85 (79.92)	72.04 (62.11)	5.59 (3.37)	33.18 (24.98)	4.48 (3.18)	5.05 (4.75)	4.97 (3.93)	4.18 (2.88)
C	3.76 (7.09)	9.78 (17.08)	36.14 (44.02)	14.78 (22.54)	28.18 (40.46)	13.62 (25.90)	15.64 (24.75)	30.49 (42.00)
O	8.15 (11.54)	13.92 (18.24)	32.00 (29.26)	40.61 (46.47)	36.30 (39.11)	19.00 (21.14)	43.59 (51.74)	32.99 (34.08)
P	1.05 (0.77)	1.78 (1.20)	2.84 (1.34)	– –	6.96 (3.88)	19.65 (14.48)	14.89 (9.12)	9.29 (5.00)
Ca	0.92 (0.52)	1.40 (0.73)	1.95 (0.71)	3.15 (1.44)	7.14 (3.07)	23.22 (13.23)	18.64 (8.85)	12.64 (5.22)
Na	–	–	0.89 (0.57)	0.81 (0.64)	7.73 (5.80)	– –	1.34 (1.11)	1.35 (0.97)
Cl	–	–	0.79 (0.33)	6.20 (3.21)	8.88 (4.31)	13.50 (8.70)	0.92 (0.49)	0.98 (0.46)
S	–	–	0.45 (0.21)	1.27 (0.72)	0.32 (0.17)	0.43 (0.3)	– –	0.16 (0.08)
N	–	–	19.34 (20.20)	– –	– –	– –	– –	7.92 (9.35)

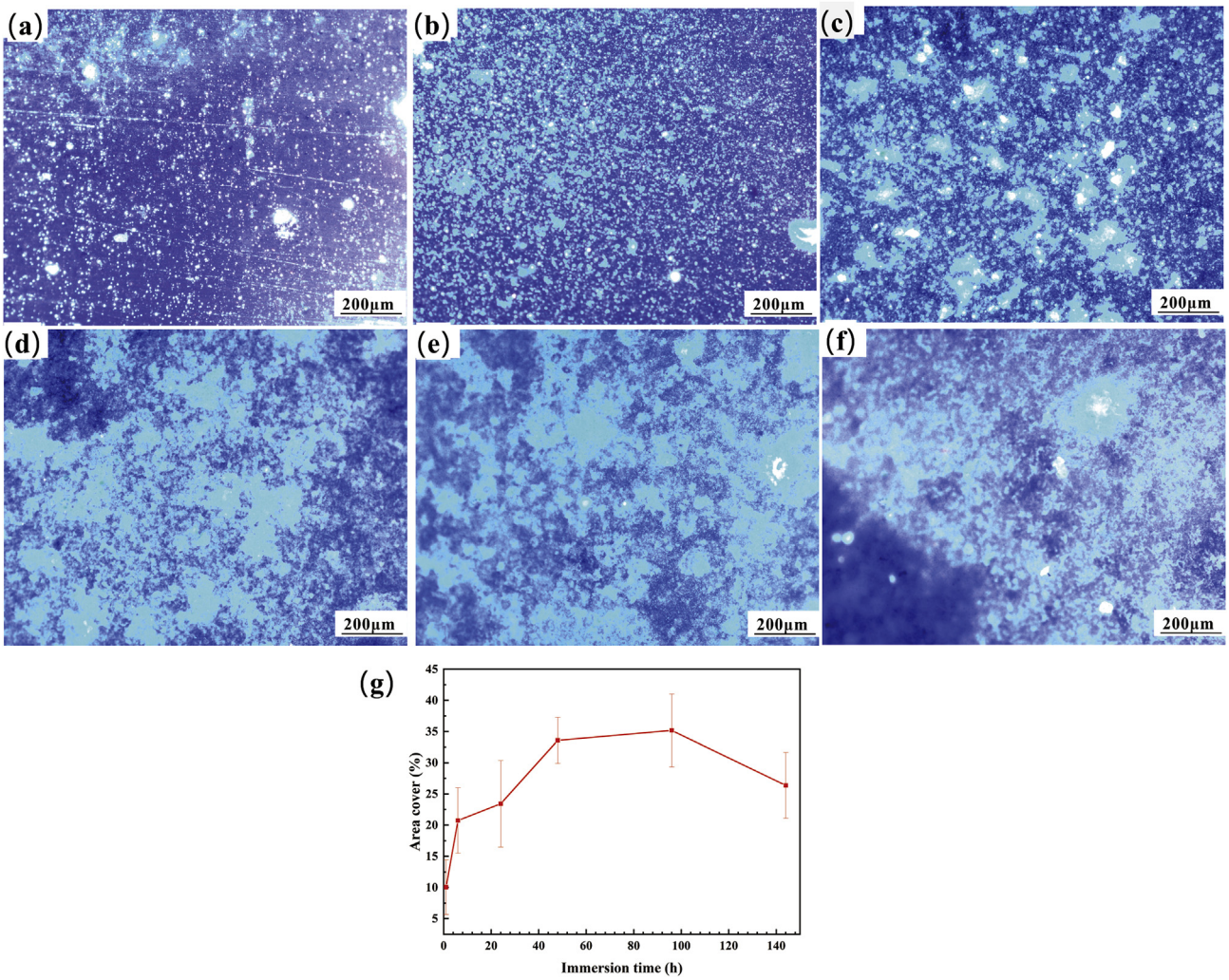

Fig. 2. Fluorescence microscopy (a–f) and corresponding bacterial adhesion in percent area (g) of Mg–1Li–1Ca alloy immersed in Hank's solution with the presence of 1 g/L glucose for (a) 1 h, (b) 6 h, (c) 24 h, (d) 48 h, (e) 96 h and (f) 144 h.

indistinct. When the immersion time was prolonged to 168 h, rod-like bacteria colonies seemed visible again. The content of N in spectrum #8, lower than that of spectrum #3, revealed that bacterial activity still influences the degradation process.

Fig. 2 depicts fluorescence microscopy and corresponding bacterial adhesion in percent area of Mg–1Li–1Ca samples immersed in Hank's solution for 1 h, 6 h, 24 h, 48 h, 96 h and 144 h. The activity of bacterial attachment, growth, reproduction and biofilm formation can be seen from the immersion test. Most of the bacteria were monomer and local bacterial colonies were attached after immersion in 1 h (Fig. 2a). Then, a dynamic process occurred approximately from 6 to 48 h (Fig. 2b–d) that bacteria inhomogeneously agglomerate together, with extracellular polymeric substances (EPS), to form biofilm on the sample surface. The percent of bacterial adhesion area was increased to 33.59% ± 3.69% (Fig. 2g). The result is attributable to that the adequate oxygen and nutrients (i.e. glucose) make the bacteria activities strongly, which produced more bacteria metabolites and contributed acidification tendency of the solution. It was noted that after 96 h immersion, the attached bacterial colonies (Fig. 2e) slightly increased, but then it dropped from 144 h (Fig. 2f). This implies that after approximately 96 h immersion, microbial growth has gone decline. Accordingly, bacterial adhesion in percent area was decreased from 35.18% ± 5.85%–26.39% ± 5.28% (Fig. 2g).

Fig. 3 shows tensile stress-strain curves (a) and tensile mechanical properties (b) of Mg–1Li–1Ca substrate after immersion in Hank's solution for 0 days, 1 d, 2 d, 4 d and 7 d. The alloy exhibited the highest ultimate tensile strength (UTS) with a value of 181.5 ± 1.3 MPa. After an immersion in Hank's solution for 1 d, 2 d, 4 d and 7 d, UTS decreased to 166.0 ± 5.2 MPa, 158.0 ± 4.2 MPa, 157.0 ± 9.1 MPa and 157.0 ± 5.0 MPa, respectively. The yield strength (YS) was significantly reduced after immersion for 1 d due to the attached bacteria, while moderately decreased after 2 d, 4 d and 7 d immersion. The elongation (EL) to failure of the alloy was 13.2 ± 0.4%. After immersion, EL decreased to 8.2 ± 0.9% (1 d), 6.9 ± 0.3% (2 d), 7.0 ± 1.2% (4 d), 6.8 ± 0.7% (7 d). That is, toughness of the alloy markedly declined with time. This finding might be ascribed to hydrogen brittle or delayed hydride cracking [32,33].

XRD patterns of Mg–1Li–1Ca substrate before and after immersed in the solution for 168 h is shown in Fig. 4a. In addition to the dominant peaks corresponding to α-Mg phase, some peaks at approximately 2θ = 18, 38° correspond to the wide diffraction peaks of amorphous Mg $(OH)_2$. It is noting that the peaks (2θ = 28, 31, 70°) of Mg_2Ca phase disappeared after the immersion due to Mg_2Ca phase acted as an efficient anode with lower potential for hydrogen evolution [34]. FTIR analysis (Fig. 4b) was further carried out to verify the effect of bacteria activity in the corrosion process. Typically, the solution within immersed Mg–1Li–1Ca substrate was also studied. The sharp but weak peak at 3700 cm^{-1} corresponds to Mg–OH stretching vibrations. The broad absorption band at around 3300 cm^{-1} is attributed to OH or N–H [35]. The band at about 2929 cm^{-1} can be ascribed to the bending

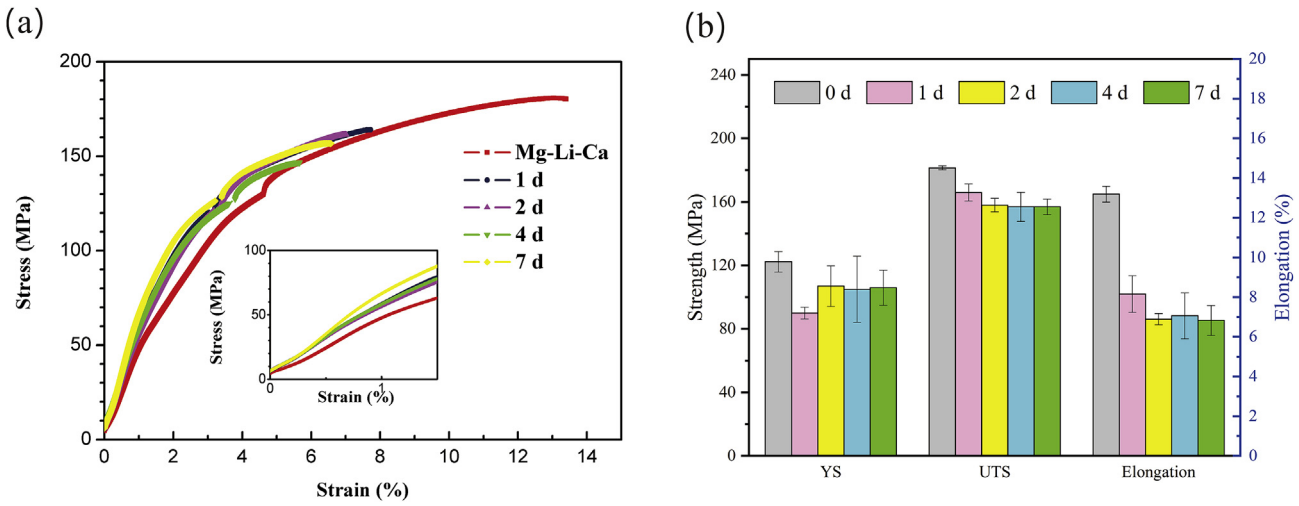

Fig. 3. Tensile stress-strain curves (a) and tensile mechanical properties (b) of Mg–1Li–1Ca substrate after immersion in Hank's solution for 0 d, 1 d, 2 d, 4 d and 7 d.

vibration of C–H of CH_2 in fatty acids [36,37]; whereas the bands at 1737 cm^{-1} and 1654 cm^{-1} can be related with the stretching vibration of C═O in nucleic acids and amide I [38]. The characteristic band at 1419 cm^{-1} can be assigned to the stretching vibration of COO^- ions due to transformation of glucose into glucose acid [3]and the component of amino acids [39]. Moreover, the absorption around 1053 cm^{-1} and 565 cm^{-1} are typical for PO_4^{3-} ions, designating the formation of phosphoric acid product. In Hank's solution, the band at around 1567 cm^{-1} and 1249 cm^{-1} originates from amide II and amide III [40], which is the combination of C–N bending and N–H bending in proteins or amino acids. In a word, It further demonstrates the existence of bacterial activity.

To better understand the effect of bacteria activity and biofilm adhesion, XPS analyses were performed for the sample surface immersed in Hank's solutions for different times (1, 2, 4, 7d). The results are in good agreement with the aforementioned FTIR results. C 1s and N 1s spectra of the samples are presented in Fig. 5, Fig. 6 and respectively. The C 1s spectra of the sample which immersed 1 d (Fig. 5a) can be split into three peaks. The peaks can be attributed to C–C, C═O and C-(O, N) bonds [41]. The new peak at 289.2 eV was observed that can be associated with the –COOH, which replace the peak related to the C═O bond after immersed 2 d (Fig. 5b), revealing the transformation of glucose into gluconic acid [42], which is the carbon resource of bacteria. What's more, a new peak at 285.6 eV is can be associated with the C–N group after immersed 4 d (Fig. 5c). This indicates that microbial metabolites exert a considerable influence after active growth and reproduction in 2 d.

Fig. 6a–d demonstrates the curves fits of N 1s spectra for the samples after immersion in Hank's solutions for various periods. The N 1s spectra of 1 d (Fig. 6a) is split into two peaks. The peak at 399.1 eV can be assigned to the C–N bond. The peak at 400 eV can be attributed to the $–NH_2$ bond. However, three peaks were observed at 401.1 eV that could be attributed to the -N-C═O group after immersed 2 d (Fig. 6b). The presence of N, does not contain N element in Hank's solution, further implies the existence of bacterial activity on Mg surface during *in vitro* experiment. XPS results revealed that the biofilm formed on the magnesium alloys was composed of EPS and clusters of bacteria cells. The large proportion of C–O bonds in the C 1s spectra were believed to arise from extracellular polysaccharides, which are major components of EPS [43]. Additionally, the transformation from –C═O to –COOH may be an important factor of pH unusual acidification process and further affect the corrosion mechanism.

After the above discussion, we know that microorganisms enormously influence the degradation behavior of the magnesium in Hanks's solution. Therefore, microbial community diversity in immersion solution based on metagenomics was performed. The dominant

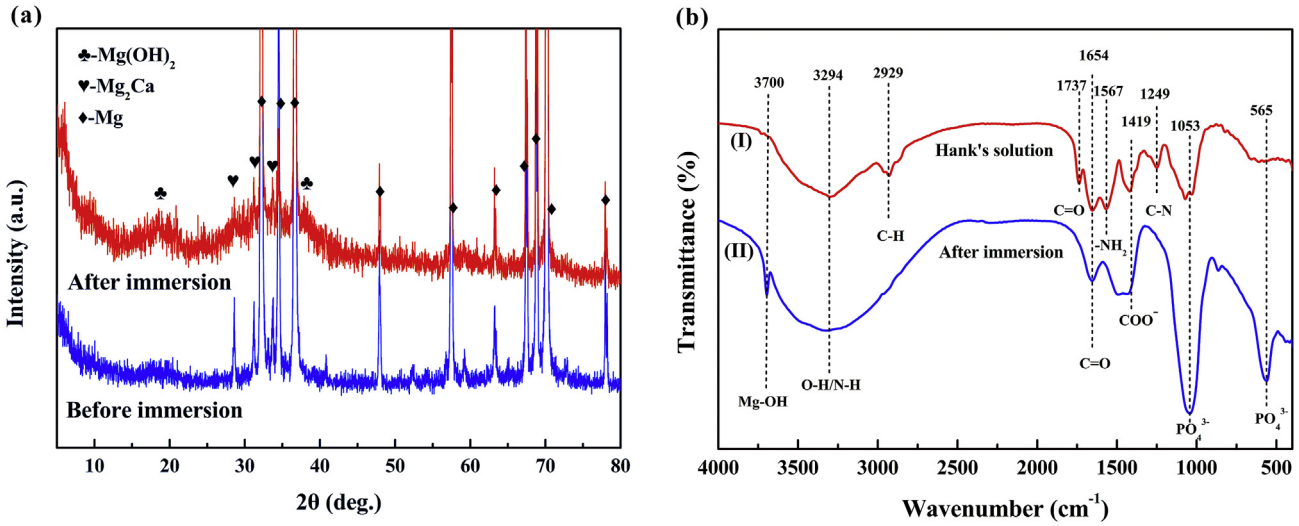

Fig. 4. (a) XRD patterns of Mg–1Li–1Ca substrate before and after immersion in Hank's solution for 168 h. (b) FTIR spectra of (I) Hank's solution and (II) Mg–1Li–1Ca sample immersed in Hank's solution for 168 h.

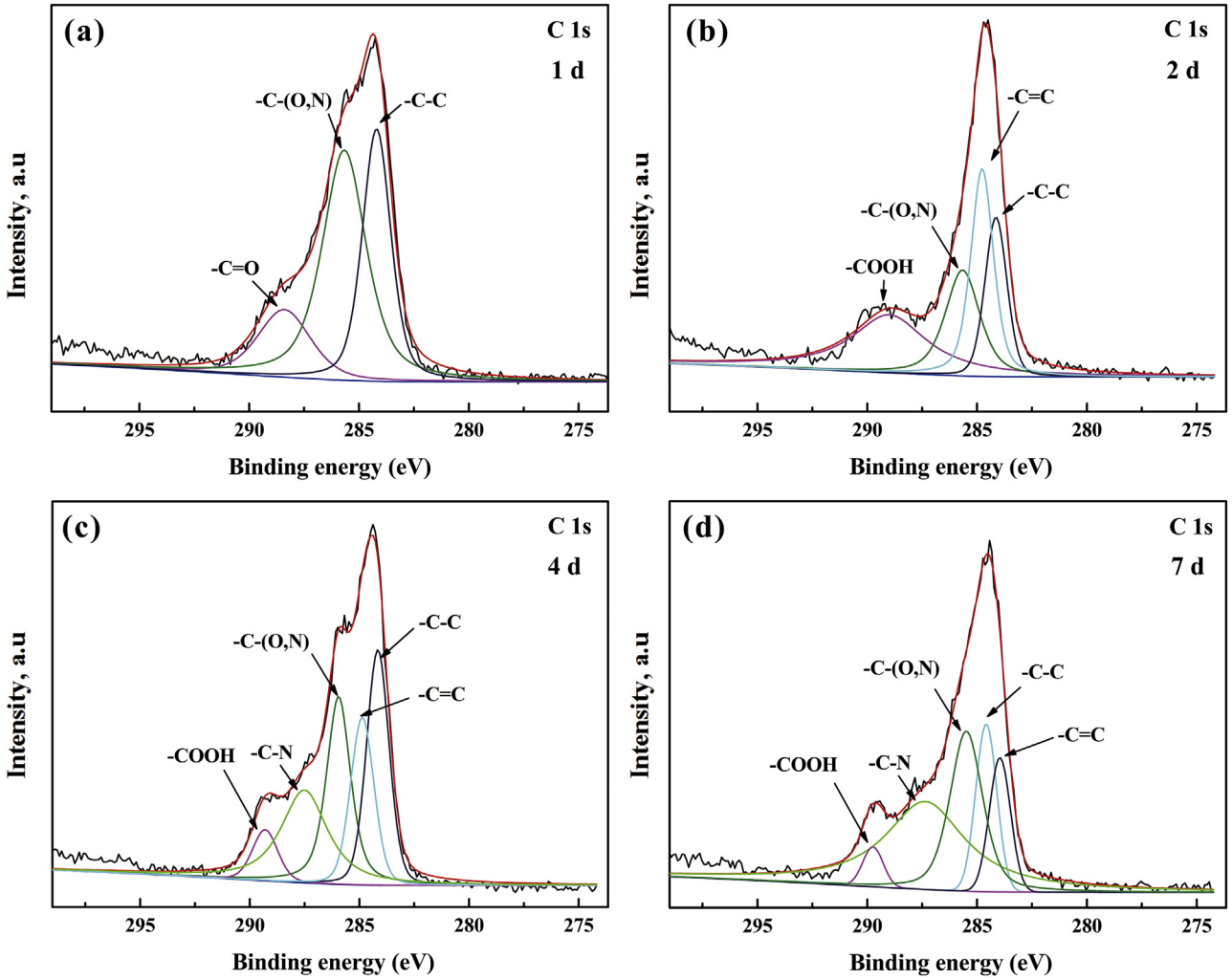

Fig. 5. XPS analysis of Mg–1Li–1Ca surface after immersion in Hank's solutions for various periods. C 1s spectra for (a) 1 d, (b) 2 d, (c) 4 d and (d) 7 d.

members of the bacteria community that pollute the Hank's solution were identified using *16S rRNA* method (Fig. 7f). The bacteria include the genera Pseudomonas (54.08%), Paenibacillus (16.58%), Anaerobacter (6.70%), Flavobacterium (3.63%), Rhizobium (3.53%), Bacillus (3.03%), Anaerosinus (2.39%), Azomonas (2.16%), Azospirillum (1.53%), and the other (6.37%). On the other hand, Strains *Gordonia terrae* NBRC 100016 (Fig. 8a), *Pseudomonas stutzeri* ATCC 17588 (Fig. 7b), *Microbacterium hominis* IFO 15708 (Fig. 7c), *Enterobacter xiangfangensis* DSM 14472 (Fig. 7d) and *Bacillus nealsonii* DSM 15077 (Fig. 7e) five kinds of bacteria extracted from the immersion solution via spread plate and streak plate methods.

Notably, there are two kinds of acid-producing bacteria *Microbacterium hominis* IFO 15708 and *Enterobacter xiangfangensis* DSM 14472. Both of them can consume glucose etc. to produce acidic metabolites [44–46]. Hank's solution with 1 g/L glucose was used *in* this *vitro* experiment. It is hypothesized herein that glucose could be the reason for acidification of solution and the organic carbon resource of bacterial activity. Therefore, investigations in Hank's solution without glucose were carried out to make a fully understanding of this mechanism.

3.2. Investigations in glucose-free Hank's solution

Fig. 8 illustrates pH values and hydrogen evolution rate (HER) of Mg–1Li–1Ca samples in Hank's solution with and without glucose. As previously discussed, pH values in Hank's solution with glucose (Fig. 8a) firstly increased and decreased to around 5.0, and then continuously increased, which can be ascribed to the acidic metabolites resulted from bacterial activity. Interestingly, it is in glucose-free Hank's solution that the pH value slightly rose in the first day's immersion and then maintained a stable alkaline environment. Simultaneously, HER in glucose-free Hank's solution (Fig. 8b) marginally increased, and then keeps a slow decrease and finally static tendency corresponding to its pH value. Differently, HER in the presence of glucose in Hank's solution was low first and then rapid increased, attributing to the formation of severe acidic metabolites caused by bacterial activity. The larger amount of hydrogen released can be seen in chemical reaction (3). With the extension of immersion, HER decreased with bacterial apoptosis. Thus, glucose in Hank's solution provides the major energy sources for bacterial activity. The formation of acidic bacterial metabolites markedly promoted the degradation rate of the Mg–1Li–1Ca alloy in Hank's solution.

$$Mg\ (s)\ +\ 2H^{+} \rightarrow Mg^{2+}(aq)+H_2\uparrow \qquad [3]$$

The SEM morphologies of Mg–1Li–1Ca samples in glucose-free Hank's solution for different time (24, 48, 96, 168 h) are displayed in Fig. 9. As shown in Fig. 9a, the samples were subjected to corrosion and a layer of corrosion products with cracks formed. After immersion in 48 h (Fig. 9b), corrosion products with more randomly distributed spherical particles were observed on sample surface. With the extension time to 96 h (Fig. 9c), corrosion products deposited on the surface inhomogeneously. While it lasted up to 168 h (Fig. 9d), an thick and

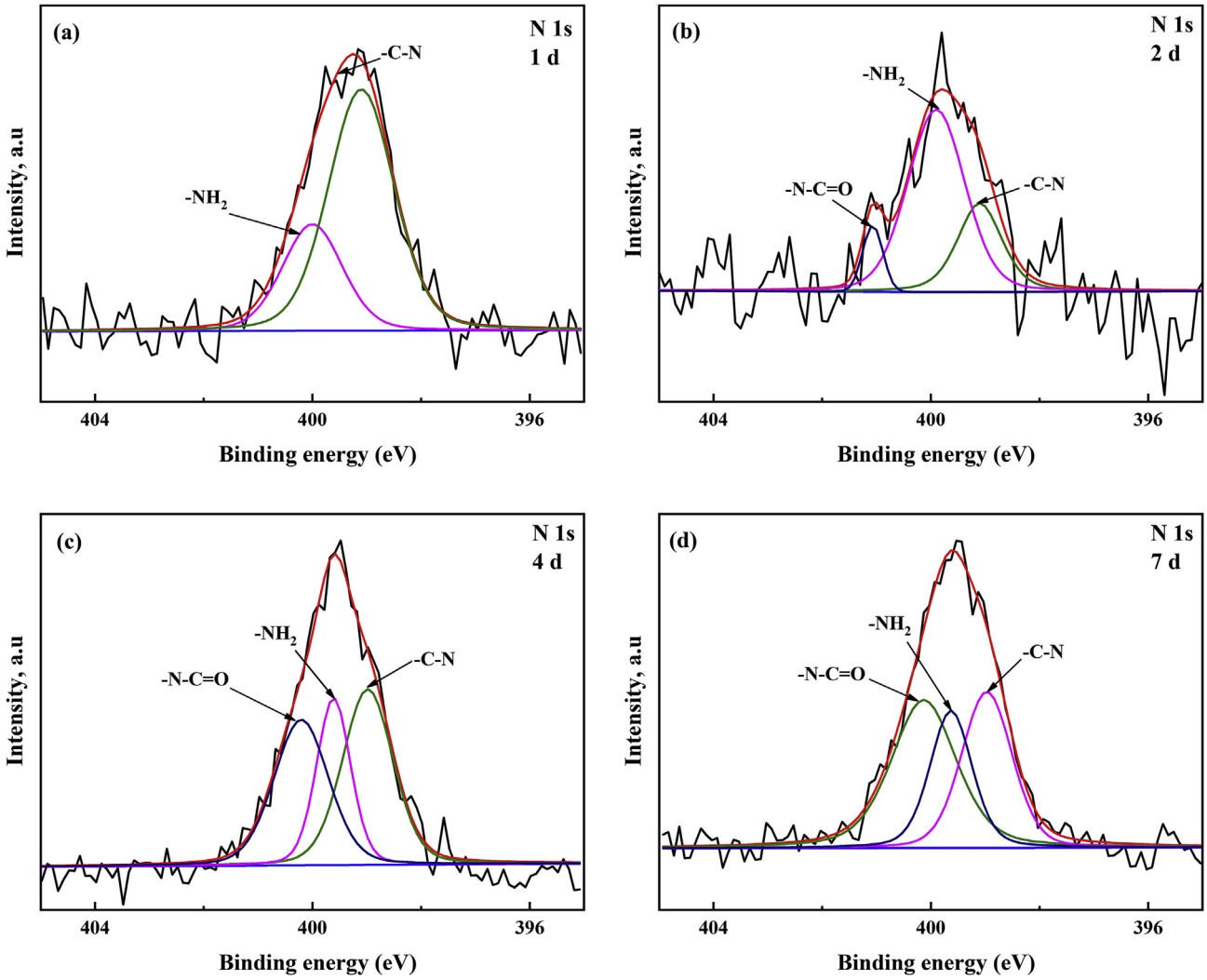

Fig. 6. XPS analysis of Mg–1Li–1Ca surface after immersion in Hank's solutions for various periods. N 1s spectra for (a) 1 d, (b) 2 d, (c) 4 d and (d) 7 d.

dense layer of bacterial colonies was completely covered on the sample surface. Surprisingly, small bacterial colonies might exist.

The corresponding EDS analyses, listed in Table 2, can identify the existence of bacteria. In the first immersion time of 96 h (Spectrum #1–6), Ca and P elements are unevenly distributed on the sample surface, which in raised part such Spectrum #3, 6 have higher concentration, disclosed Ca–P corrosion products discretely formed on sample surface. It was not until 168 h immersed in free-glucose Hank's solution that the N element was detected (Spectrum #7–8), indicating that the absence of glucose in Hank's solution retarded the activity of bacterial. A trace of S element was also detected on the sample surface (Spectrum #1, 5 and 6). Furthermore, Ca and P contents were relatively uniform on the sample surface, which might relate to bacterial activity, which promoted the formation of calcium phosphate products. In comparison, the content of S and N element presented significantly lower than in Hank's solution with 1 g/L glucose (Table 1), indicating the inhibition of bacterial activity under glucose-free condition.

Fig. 10 depicts the FTIR spectra and XRD patterns of Mg–1Li–1Ca substrate after exposure to glucose-free Hank's solution for different time. In FTIR spectra (Fig. 10a), the peaks of Mg–OH, O–H, CO_3^{2-} and PO_4^{3-} were observed on the sample surface, without organic components, such as C═O, COO-, N–H, revealed that bacterial activity was substantially decreased. Different from in Hank's solution, the XRD results (Fig. 10b) in glucose-free Hank's solution showed that more Ca–P corrosion products are deposited on the sample surface. It is noting that the intensity of DCPD ($CaHPO_4{\cdot}2H_2O$) was highest in 1d immersion. Afterwards the intensity of DCPD decreased in 2 d and 4 d immersion, but enhanced in 7 d, which is good agreement with the EDS analysis.

Fig. 11 designates the curves fits of C 1s spectra for Mg–1Li–1Ca samples after immersion in glucose-free Hank's solutions for various periods (a) 1 d, (b) 2 d, (c) 4 d and (d) 7 d. When immersion for 1 d (Fig. 11a), the C 1s spectra can be divided into three peaks: C–C is detected at around 284.3 eV, C–O can be found at 285.1 eV and the other relatively weak signal of –COOR (288.4 eV) may be attributed to bacterial metabolites [47]. In addition to C–C, C–O and –COOR group, a new peak after immersion for 2 d (Fig. 11b) at 284.6 eV was observed that associated with C-(O, N) group [48]. However, when immersion time prolonged to 4 d (Figs. 11c) and 7 d (Fig. 11d), the peak of C-(O, N) group was disappeared. This indicates that the bacterial activity is very active at 2 d immersion.

This part mainly focuses on the roles of glucose in the degradation of Mg alloys to make sure the factors that caused abnormal acidification in Hank's solution. According to the above results, it will not lead to acidification of solutions without glucose, but the emerge of bacterium latter should not be neglected.

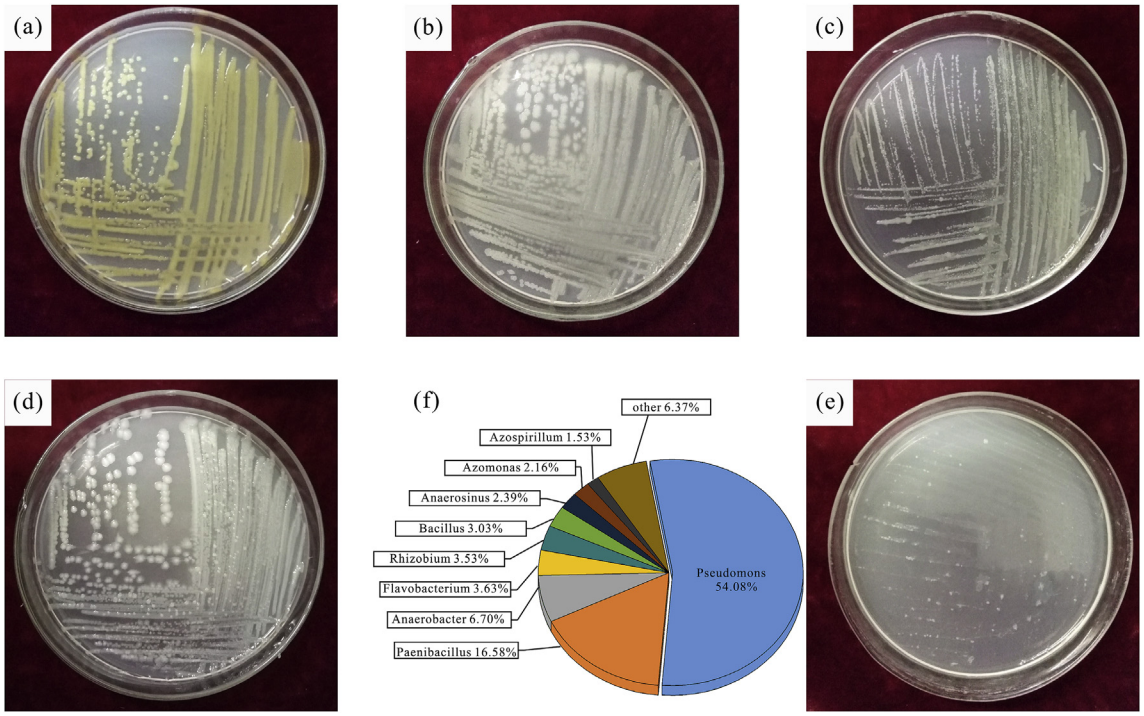

Fig. 7. Bacteria isolated from the immersion solution, identified by 16S rRNA gene analysis. (a) *Gordonia terrae* NBRC 100016, (b) *Pseudomonas stutzeri* ATCC 17588, (c) *Microbacterium hominis* IFO 15708, (d) *Enterobacter xiangfangensis* DSM 14472, (e) *Bacillus nealsonii* DSM 15077 and (f) Distribution of the most abundant genera in the samples.

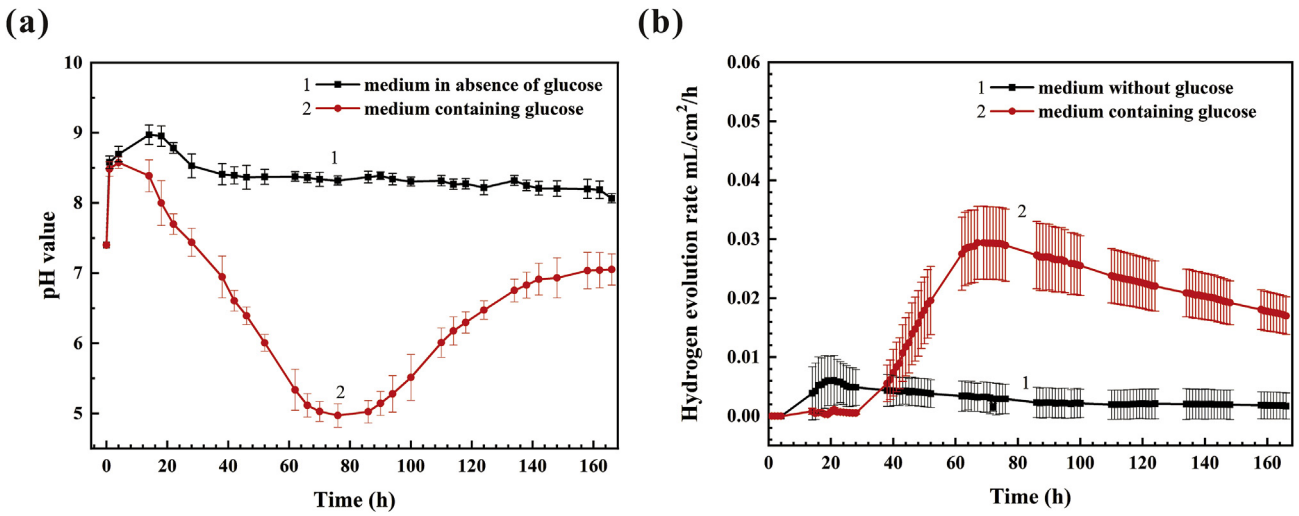

Fig. 8. (a) The pH values and (b) hydrogen evolution rate (HER) of Mg–1Li–1Ca samples immersed in Hank's solution (medium containing glucose) and glucose-free Hank's solution (medium without glucose).

3.3. Influence of Microbacterium hominis and Enterobacter xiangfangensis in Hank's solution

The hydrogen evolution rates (HER) and pH values vs. immersion time curves of the samples with two kinds of acid producing bacteria in Hank's solution are displayed in Fig. 12. It was confirmed that the bacteria activity acidifies the Hank's solution. They all showed the pH value decrease during the immersion test. Due to the different kinds of bacteria competed in the Hank's solution, the pH value of Hank's solution has different low points to the others. But the acidy solution accelerated magnesium corrosion rates.

Fig. 13 shows Mg–1Li–1Ca samples immersed in Hank's solution (Fig. 13 a1∼a4), Hank's solution containing about 10^9 CFU *M. hominis* (Fig. 13 b1∼b4) and Hank's solution containing about 10^9 CFU *E. xiangfangensis* for different corrosion stages (24 h, 48 h, 96 h and 168 h). Microbiologically-influenced corrosion occurred on Mg alloys at ambient temperature in laboratory. Bacteria can be found in the magnesium surface after immersed 24 h in the Hank's solution (Fig. 13 a1) and Hank's solution containing *E. xiangfangensis* (Fig. 13 c1). Bacteria adhered the samples surface after Mg alloys samples immersed in Hank's solution containing *M. hominis* (Fig. 13 b1) after 48 h. The corrosion pits grew quickly when pH value became lower. After 48 h of immersed in Hank's solution, a number of bacteria adhered to the Mg alloys surface. Because amount of bacteria multiply metabolism, the bacteria and their EPS formed the biofilm on the Mg alloys surface. At 168 h, due to the consumption of nutrients and unsuited acidic condition, parts of the bacteria biofilm fell off from the Mg alloys surface.

The FTIR results of samples after immersion in Hank's solutions

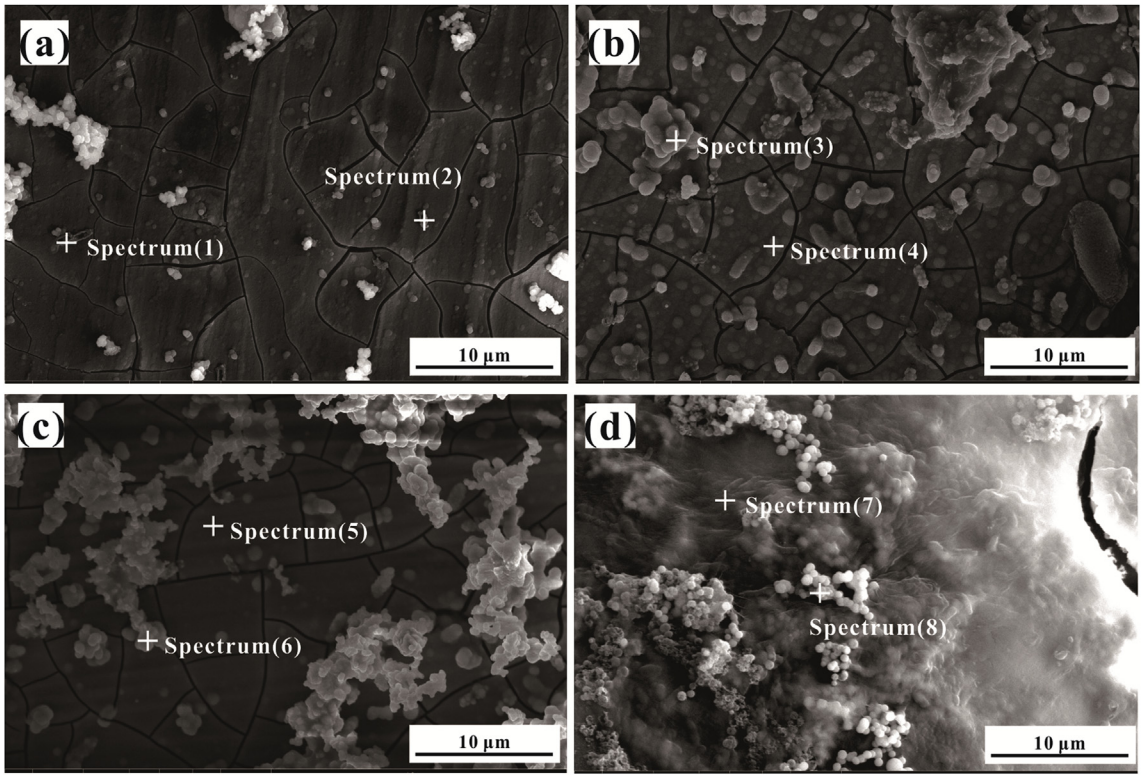

Fig. 9. SEM morphologies of Mg–1Li–1Ca after immersion in glucose-free Hank's solution for different time. (a) 24 h, (b) 48 h, (c) 96 h, (d) 168 h.

containing different bacteria are displayed in Fig. 14 (a). And the FTIR results of Hank's solution containing different bacteria are demonstrated in Fig. 14 (b). The absorption bands at 3726 cm^{-1} and 3463 cm^{-1} corresponding to O–H stretching vibrations. A band at approximately 3693 cm^{-1} corresponding to Mg–OH stretching vibrations revealed the existence of $Mg(OH)_2$. The band at 2920 cm^{-1} can be ascribed to the bending vibration of $–CH_2$ in fatty acids. The bands at 1737 cm^{-1} and 1650 cm^{-1} can be related with the stretching vibration of C═O in nucleic acids and amide I. The absorption at 1438 cm^{-1} related to CO_3^{2+} ions. The characteristic bands assigned to the stretching vibration of $–CH_2$ are found at 1420 cm^{-1} and 1250 cm^{-1}. Meanwhile, the absorption bands at 1036 cm^{-1},1053 cm^{-1} and 573 cm^{-1} are related to the PO_4^{3-} ions.

4. Discussion

In present work, the effects of glucose on unusual pH value for Mg–1Li–1Ca Mg alloy in Hank's and glucose-free Hank's solution were systematically investigated, respectively. The result exhibited that the abnormal acidification of Hank's solution for Mg–1Li–1Ca Mg alloy was caused mainly by bacterial activity. Bacterial activity in immersion test is an extremely complex process that is affected by many factors, such as, carbon resource [49], temperature [50], antibiotics [51] and concentrations of electrolytes [19]. Better understanding of the interaction between bacteria and Mg alloys is of significance. The developmental process of bacterial activity in immersion test can be summarized for three stages (Fig. 15), starting with surface attachment, followed by

Table 2
EDS analysis data of Mg–1Li–1Ca alloy immersed in glucose-free Hank's solution in Fig. 9 in wt.% (at. %).

Elements	Spectrum							
	#1	#2	#3	#4	#5	#6	#7	#8
Mg	47.17 (79.92)	68.48 (60.58)	4.52 (3.61)	80.41 (74.85)	79.07 (72.61)	9.48 (9.03)	20.53 (20.15)	8.47 (7.48)
C	– –	7.32 (13.10)	11.70 (18.89)	4.43 (8.35)	3.42 (6.37)	– –	–	–
O	23.47 (34.84)	15.47 (20.80)	46.85 (56.79)	9.12 (12.91)	13.03 (18.18)	38.85 (56.23)	26.79 (39.96)	43.91 (58.18)
P	5.77 (4.43)	3.80 (2.64)	14.33 (8.97)	2.71 (1.98)	1.81 (1.31)	19.71 (14.76)	14.56 (11.21)	14.24 (9.74)
Ca	18.50 (10.96)	3.72 (2.00)	18.73 (9.06)	2.88 (1.63)	1.95 (2.05)	25.38 (14.69)	17.19 (10.22)	17.24 (9.14)
Na	0.81 (0.83)	0.49 (0.45)	1.87 (1.58)	– –	– –	2.72 (2.75)	8.79 (9.12)	5.59 (5.15)
Cl	4.08 (2.73)	0.72 (0.44)	2.00 (1.09)	0.45 (0.29)	0.51 (0.32)	3.65 (2.38)	10.95 (7.34)	6.17 (3.68)
S	0.22 (0.16)	– –	– –	– –	0.11 (0.08)	0.21 (0.16)	–	–
N	– –	– –	– –	– –	– –	– –	1.18 (2.00)	4.38 (6.63)

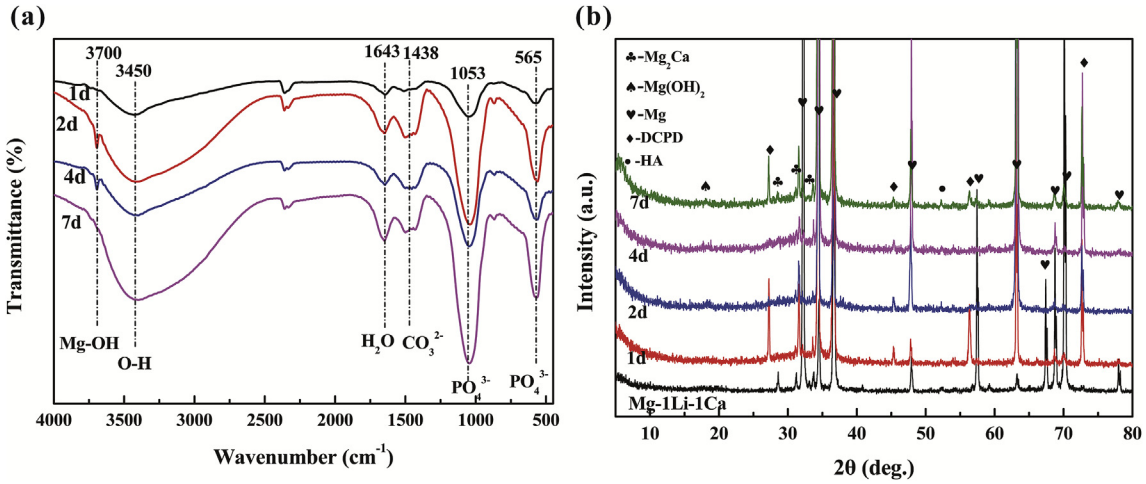

Fig. 10. FTIR spectra (a) and XRD patterns (b) of Mg–1Li–1Ca substrate after immersion in glucose-free Hank's solution for different time (1 d, 2 d, 4 d and 7 d).

multilayered bacterial cell proliferation and finally extinction with immersion time. Firstly, a small quantity of germ germinates on the surface of magnesium with a few pits. Then glucose in Hank's solution nourishes the bacteria, and some bacteria use glucose to generate acidic products, which is confirmed by fluorescence microscopy in Fig. 2. It should be noticed that it has competitive relation between colonies of various bacteria with the acidic metabolite lower the pH value of Hank's solution (Fig. 1). In the second stage, an accumulated biomass of bacteria and their EPS formed biofilm on the Mg alloy surface at approximately 48 h, exerting significant influence to corrosion behavior of Mg alloys. The existence of germ is finally restrained by unsuited acidic condition in the third stage. Thereafter, pH value would be raised by the alkaline corrosion product of magnesium in the bacterial extinction stage. What's more, in order to better understand the function of

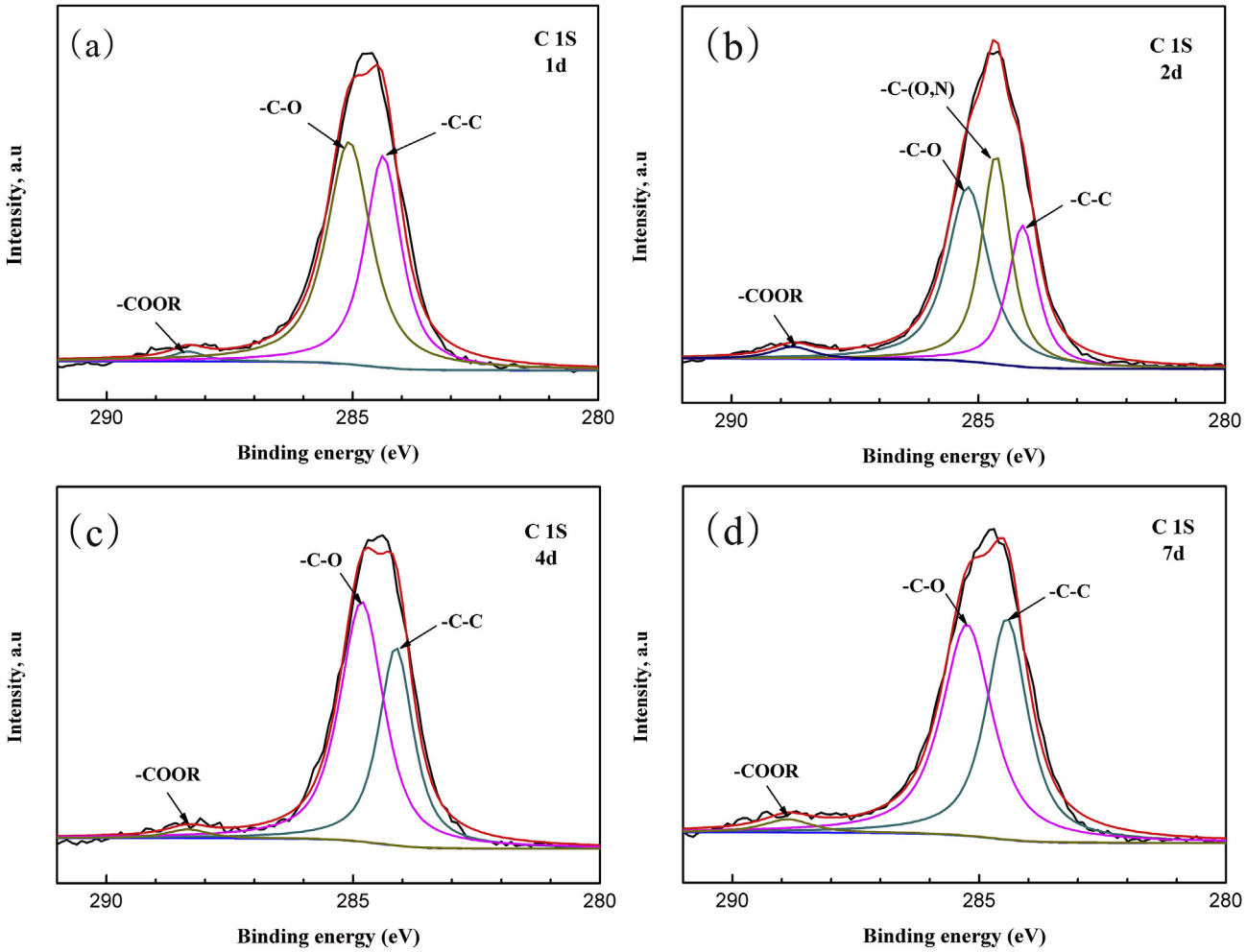

Fig. 11. XPS analysis of Mg–1Li–1Ca surface after immersion in Hank's solutions without glucose for various periods. C 1s spectra for (a) 1 d, (b) 2 d, (c) 4 d and (d) 7 d.

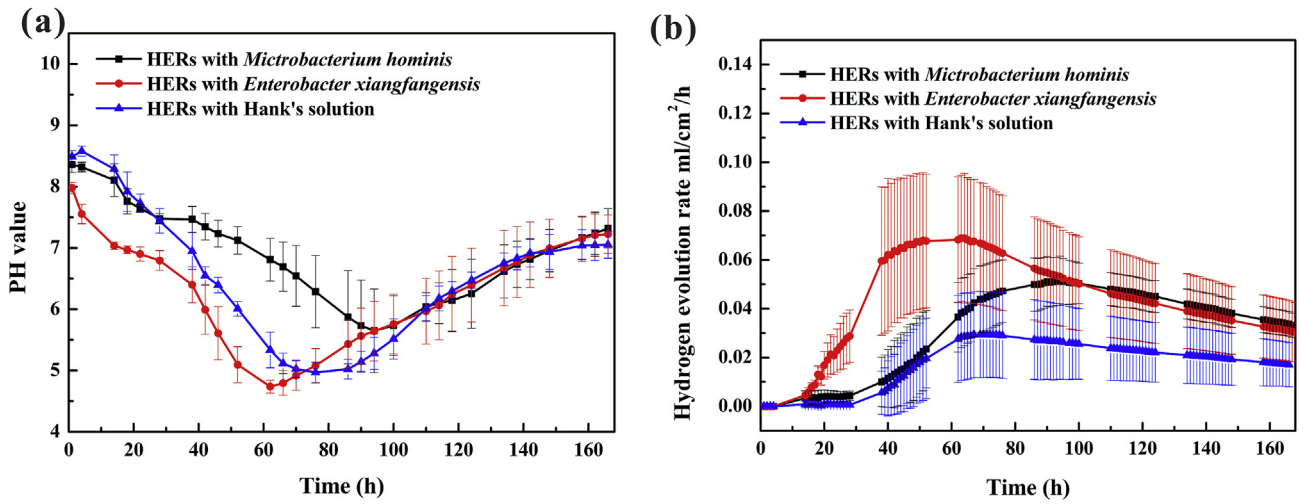

Fig. 12. The pH values (a) and hydrogen evolution rates (b) of Mg-1Li-Ca samples immersed in Hank's solution with two kinds of acid producing bacteria.

glucose in bacterial activity, explorations were also conducted in Hank's solution without glucose. The results showed that it retarded the bacterial activity without acidification of pH value (Fig. 8) for glucose-free Hank's solution.

To ascertain sources of two kinds of acid producing bacteria, *Microbacterium hominis* IFO 15708 and *Enterobacter xiangfangensis* DSM 14472, we paid much attention to previous work. Kim et al. [52] found that *Microbacterium hominis* IFO 15708 was isolated from salted turban shell. Gu et al. [53] investigated that *Enterobacter xiangfangensis* sp. nov., was isolated from Chinese traditional sourdough. The origin of

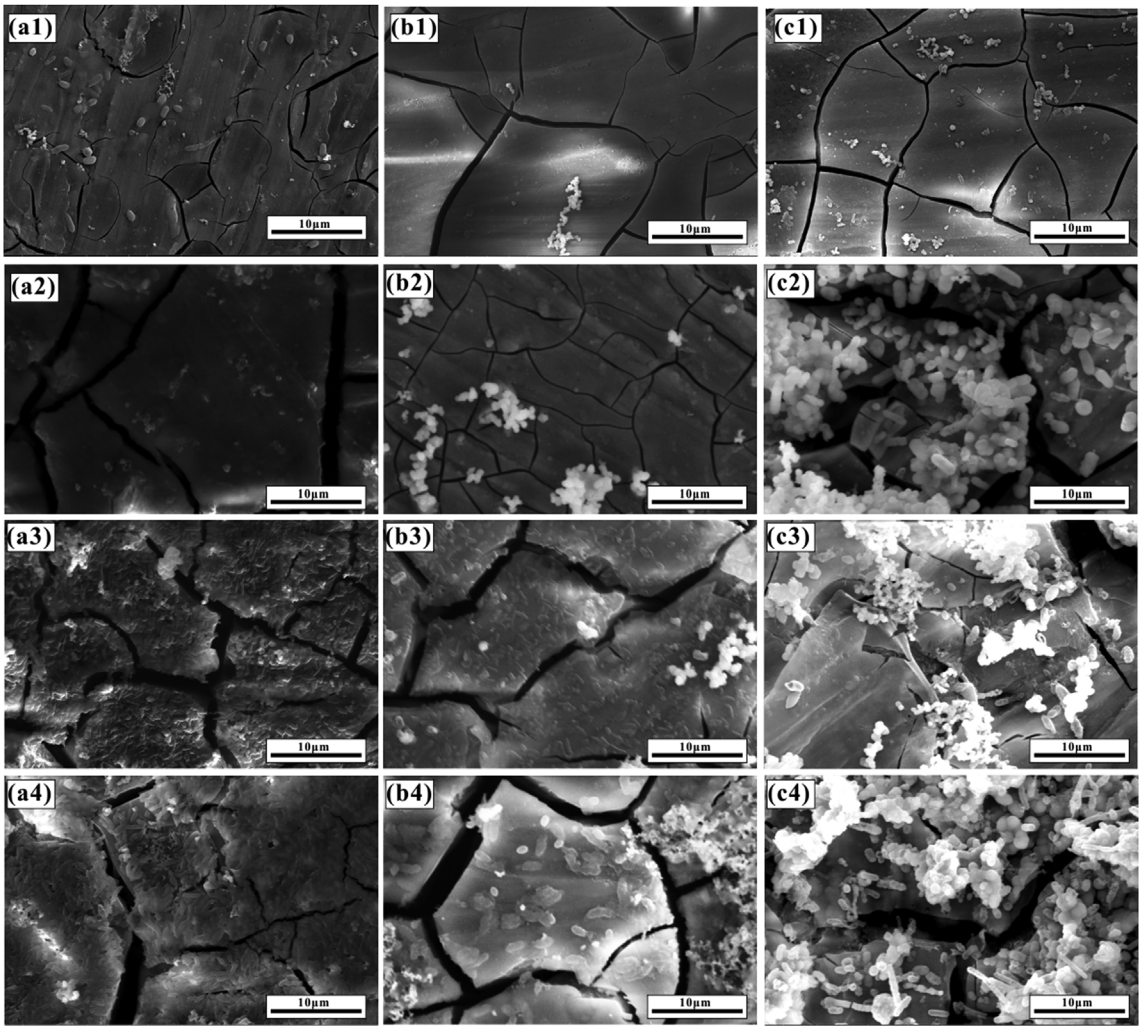

Fig. 13. The SEM images of Mg–1Li–1Ca immersed in Hank's solution (a1∼a4); Hank's solution containing Microbacterium hominis (b1∼b4); Hank's solution containing Enterobacter xiangfangensis (c1∼c4) for 24 h, 48 h, 96 h and 168 h.

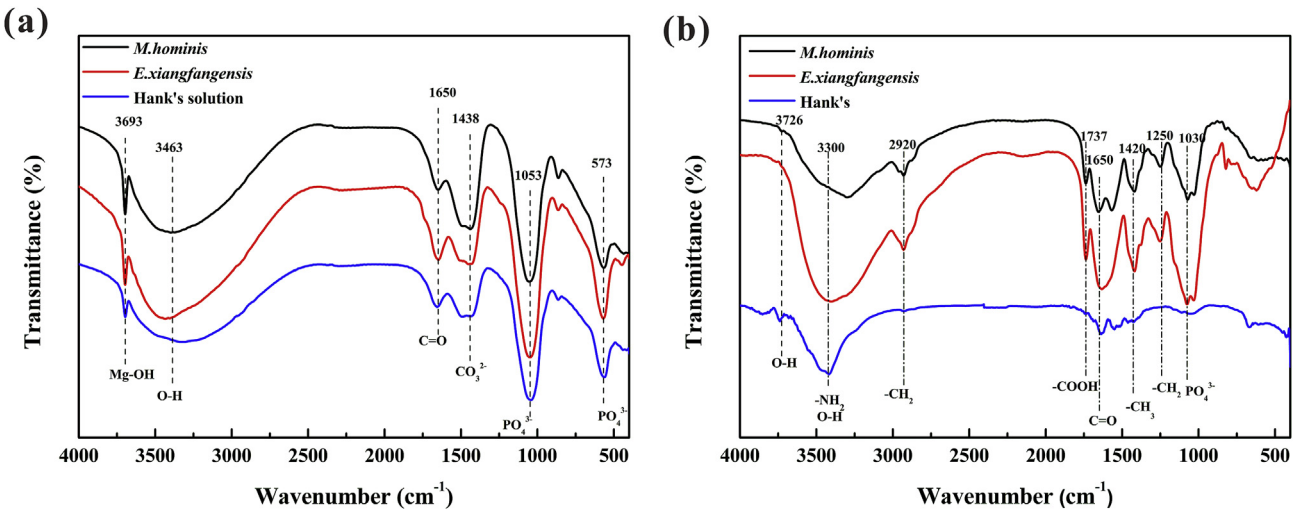

Fig. 14. The Fourier transformed infrared (FTIR) result. (a) Mg–1Li–1Ca samples after immersion in Hank's solutions (168 h) containing different bacteria and (b) the Hank's solutions containing different bacteria.

this bacterium is still unclear, but it is presumably derived from the distilled water polluted from air at high humidity environment (particularly in summer in the bath, which experience a long-term test).

On the other hand, the transformation of glucose into gluconic acid that lower pH value should not be neglected based on our previous studies [3]. It unveils that pH value initial increase with the degradation of pure Mg, then markedly decrease to around 7.7 due to the transformation of glucose into gluconic acid, rise again and finally stabilize approximately 8.5. Glucose in Hank's solution with 1 g/L glucose changes the degradation behavior of pure Mg. In contrast, the significant decrease in pH value (5.0) of Mg–Li–Ca alloy, caused by glucose and polluted distilled water, is attributed to that glucose is transformed into gluconic acid and facilitates absorption of bacterial colonies on the sample surface during immersion test. Notably, lower degradation rate of pure Mg was obtained with increasing glucose concentration in Hank's solution, which ascribed to glucose acid coordinate with Ca^{2+} ions and thus form Ca–P compounds on Mg substrates. However, 1 g/L glucose in Hank's solution promotes degradation process of Mg–Li–Ca alloy, implying that bacterial activity is superior to glucose acid function.

Glucose in Hank's solution promote the bacterial activity and increase the degradation rate of Mg–1Li–1Ca alloy. As for mechanical properties (Fig. 3), it decreases in the former 2 d immersion and subsequent keeps almost stable, which related to corrosion products given protection to the samples. Towards this unusual degradation behavior of Mg alloys caused by bacterial activity, several strategies have been proposed to mitigate the interference of germ, including the use of antibiotic and the periodic renewal of Hank's solution. The attempt was

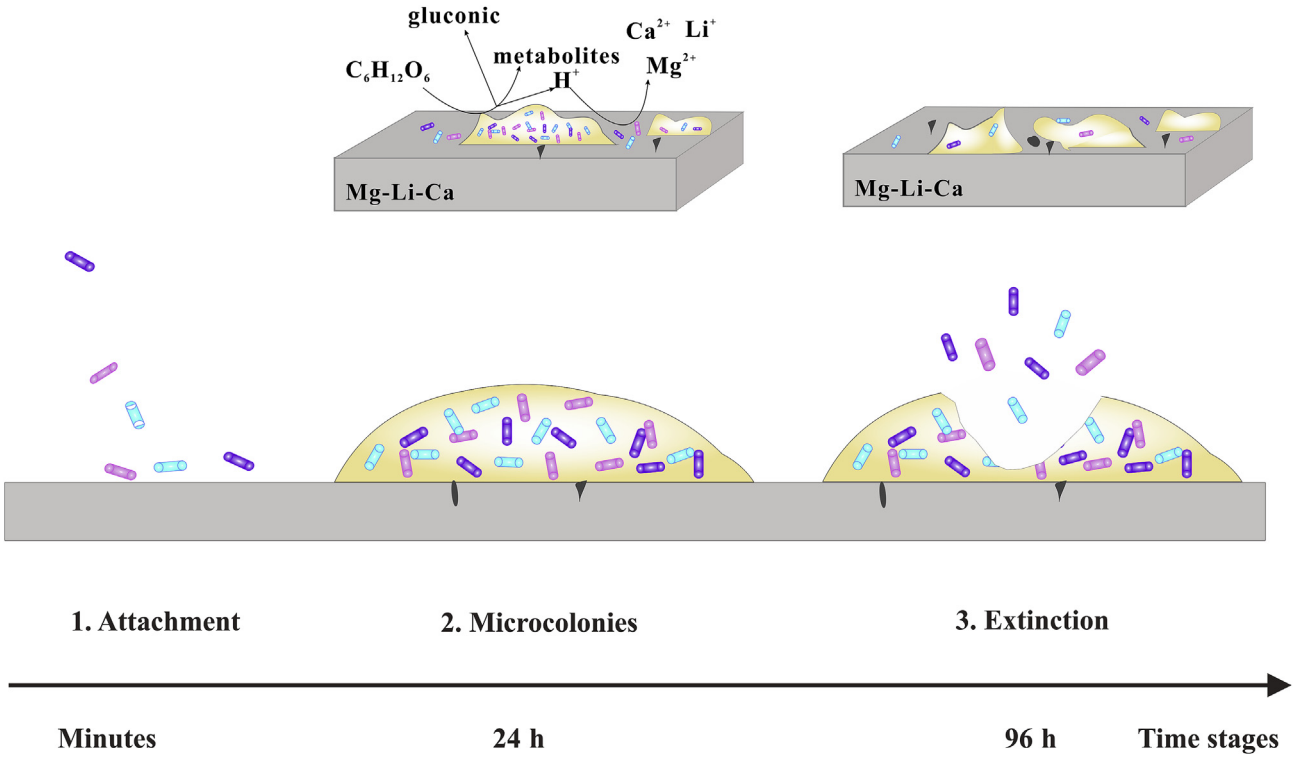

Fig. 15. Illustration of the corrosion mechanism of bacteria.

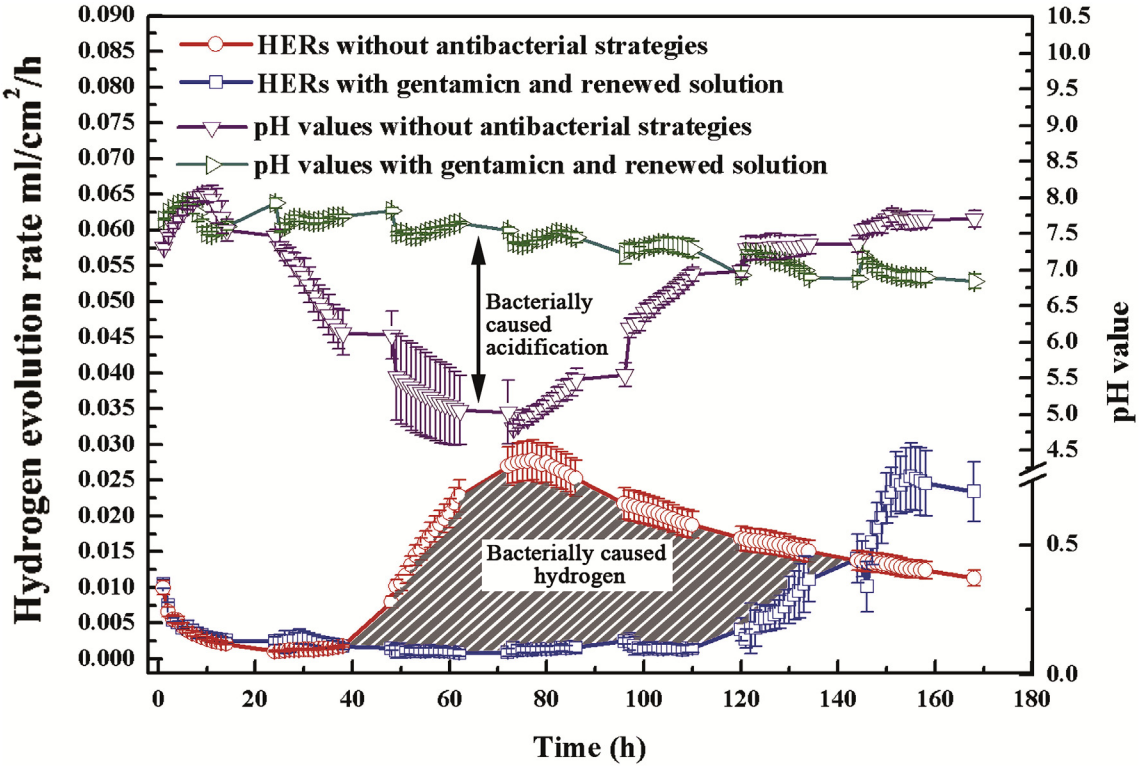

Fig. 16. The hydrogen evolution rates (HERs) and pH values of Mg–1Li–1Ca sample immersion in Hank's solution without antibacterial strategies and with gentamicin renewed every day.

displayed in Fig. 16. Renewed Hank's solution once a day with 1–1.7 mg/L gentamicin (a common board-spectrum antibiotic for cell culture) was trying to solve this problem. The growth of bacteria led to decreased pH value and acidification of solution, subsequently accelerating the degradation of Mg–1Li–1Ca alloy. The acreage of grey hatched area (Fig. 16)represents the additional hydrogen evolution, which caused by the birth of bacteria. This difference of degradation rates between samples with and without antisepsis are remarkable. It shows that HERs keep a relatively low level with the corrosion of Mg alloys at initial 120 h, while the degradation of Mg would be rapidly accelerated in absence of glucose and renewal solution. Meanwhile, the regular renewal of Hank's solution would delay the occurrence of localized corrosion [54]. Therefore, whether renewal solution with gentamicin is reasonable that still needs further exploration.

There is a series of complete operational processes during the *in vivo* test to avoid the bacterial pollution in the field of medicine, and the application of antibiotics also lower the infection risk after implanting surgery, yet standard antimicrobial treatment typically fail to eradicate biofilms [55,56]. Hydrogen evolution measurement and pH monitoring are conventional immersion tests for assessment the degradation rate of Mg implant because of their convenience and low expenditure [57]. Under normal circumstances, the human body can remain in weak alkaline condition. While local physiological pH value may be adjusted to faintly acid in some case (such as trauma and inflammation), hence this conclusion may be also appropriate for *in vivo* condition. However, material researchers have not paid much attention to the potential influence of bacteria to the result of *in vitro* test. Besides, whether the method to solve the bacterial activity is reasonable is worth further exploring.

5. Summary

This work reported that the microbiologically influenced unusual degradation behavior of biomedical Mg–1Li–1Ca alloy in immersion tests led to a decrease in pH value, acceleration in degradation rate and deterioration in mechanical properties. It is convinced that glucose in Hank's solution promoted the activities of both Microbacterium hominis and Enterobacter xiangfangensis through 16S rRNA gene analysis. Moreover, single seeded Microbacterium hominis grew faster than Enterobacter xiangfangensis in Hank's solution, which had a critical influence on degradation rate of Mg–1Li–1Ca alloy. Besides, our findings imply that a renewal solution with gentamicin might be beneficial in the eradication of bacterial adhesion and growth. Together, it enhances a growing understanding of the influence of bacterial metabolism on *in vitro* corrosion of Mg–1Li–1Ca alloy alloys and broadens our knowledge of *in vitro* degradation evaluation. Further investigations should be focused on the bacterial resource and systematic method to inhibit bacterial activity in Hank's solution for Mg alloys.

CRediT authorship contribution statement

Ling-Yu Li: Software, Formal analysis, Investigation, Data curation, Writing - review & editing. **Zhuang-Zhuang Han:** Methodology, Software, Formal analysis, Investigation, Data curation, Writing - original draft. **Rong-Chang Zeng:** Conceptualization, Supervision, Funding acquisition. **Wei-Chen Qi:** Conceptualization, Methodology. **Xiao-Fan Zhai:** Validation. **Yi Yang:** Validation. **Yun-Tian Lou:** Validation. **Tingyue Gu:** Supervision. **Dake Xu:** Supervision. **Ji-Zhou Duan:** Supervision.

Declaration of competing interest

The authors declare that they have no known competing financial interests or personal relationships that could have appeared to influence the work reported in this paper.

Acknowledgments

This work was supported by the National Natural Science Foundation of China (51571134) and Research Fund (2014TDJH104) of Shandong University of Science and Technology.

References

[1] Q. Wu, L. Wang, H.J. Yu, J.J. Wang, Z.F. Chen, Organization of glucose-responsive systems and their properties, Chem. Rev. 111 (2011) 7855–7875, https://doi.org/10.1021/cr200027j.
[2] R.M. Bergenstal, M. Johnson, R. Passi, A. Bhargava, N. Young, D.F. Kruger, E. Bashan, S.G. Bisgaier, D.J.M. Isaman, I. Hodish, Automated insulin dosing guidance to optimise insulin management in patients with type 2 diabetes: a multicentre, randomised controlled trial, Lancet 393 (2019) 1138–1148, https://doi.org/10.1016/S0140-6736(19)30368-X.
[3] R.-C. Zeng, X.-T. Li, S.-Q. Li, F. Zhang, E.-H. Han, In vitro degradation of pure Mg in response to glucose, Sci. Rep. 5 (2015) 13026, https://doi.org/10.1038/srep13026.
[4] P. Laires, K. Kurtyka, E.A. Witt, Y. Qiu, S.S. Yu, K. Iglay, Factors associated with physicians' decision to discontinue or down-titrate sulfonylureas for type 2 diabetes patients, Expert Rev. Pharmacoecon. Outcomes Res. 19 (2019) 71–79, https://doi.org/10.1080/14737167.2018.1510774.
[5] M.H.A. Muskiet, D.C. Wheeler, H.J.L. Heerspink, New pharmacological strategies for protecting kidney function in type 2 diabetes, Lancet Diabetes Endocrinol 7 (2019) 397–412, https://doi.org/10.1016/S2213-8587(18)30263-8.
[6] A. Kingston, L. Robinson, H. Booth, M. Knapp, C. Jagger, M. Project, Projections of multi-morbidity in the older population in england to 2035: estimates from the population ageing and care simulation (PACSim) model, Age Ageing 47 (2018) 374–380, https://doi.org/10.1093/ageing/afx201.
[7] L. Meng, X. Guo, X. Yang, H. Liu, M. Yu, Y. Wu, Z. Zhu, Human alpha defensins promote the expression of the inflammatory cytokine interleukin-8 under high-glucose conditions: novel insights into the poor healing of diabetic foot ulcers, J. Biochem. Mol. Toxicol. (2019) e22351, , https://doi.org/10.1002/jbt.22351.
[8] J. Zhang, H. Li, W. Wang, H. Huang, J. Pei, H. Qu, G. Yuan, Y. Li, The degradation and transport mechanism of a Mg-Nd-Zn-Zr stent in rabbit common carotid artery: a 20-month study, Acta Biomater. 69 (2018) 372–384, https://doi.org/10.1016/j.actbio.2018.01.018.
[9] C. Ke, M.-S. Song, R.-C. Zeng, Y. Qiu, Y. Zhang, R.-F. Zhang, R.-L. Liu, I. Cole, N. Birbilis, X.-B. Chen, Interfacial study of the formation mechanism of corrosion resistant strontium phosphate coatings upon Mg-3Al-4.3Ca-0.1Mn, Corrosion Sci. 151 (2019) 143–153, https://doi.org/10.1016/j.corsci.2019.02.024.
[10] Y. Su, I. Cockerill, Y. Zheng, L. Tang, Y.-X. Qin, D. Zhu, Biofunctionalization of metallic implants by calcium phosphate coatings, Bioact. Mater. 4 (2019) 196–206, https://doi.org/10.1016/j.bioactmat.2019.05.001.
[11] W. Xu, N. Birbilis, G. Sha, Y. Wang, J.E. Daniels, Y. Xiao, M. Ferry, A high-specific-strength and corrosion-resistant magnesium alloy, Nat. Mater. 14 (2015) 1229–1235, https://doi.org/10.1038/nmat4435.
[12] Z.-Q. Zhang, L. Wang, M.-Q. Zeng, R.-C. Zeng, M.B. Kannan, C.-G. Lin, Y.-F. Zheng, Biodegradation behavior of micro-arc oxidation coating on magnesium alloy-from a protein perspective, Bioact. Mater. 5 (2020) 398–409, https://doi.org/10.1016/j.bioactmat.2020.03.005.
[13] Z.-Z. Yin, W.-C. Qi, R.-C. Zeng, X.-B. Chen, C.-D. Gu, S.-K. Guan, Y.-F. Zheng, Advances in coatings on biodegradable magnesium alloys, J. Magnesium Alloys 8 (2020) 42–65, https://doi.org/10.1016/j.jma.2019.09.008.
[14] L.Y. Li, L.Y. Cui, R.-C. Zeng, S.Q. Li, X.B. Chen, Y.F. Zheng, M.B. Kannan, Advances in functionalized polymer coatings on biodegradable magnesium alloys - a review, Acta Biomater. 79 (2018) 23–36, https://doi.org/10.1016/j.actbio.2018.08.030.
[15] L.-Y. Cui, S.-C. Cheng, L.-X. Liang, J.-C. Zhang, S.-Q. Li, Z.-L. Wang, R.-C. Zeng, In vitro corrosion resistance of layer-by-layer assembled polyacrylic acid multilayers induced Ca–P coating on magnesium alloy AZ31, Bioact. Mater. 5 (2020) 153–163, https://doi.org/10.1016/j.bioactmat.2020.02.001.32.
[16] L. Wu, B.J. Luthringer, F. Feyerabend, A.F. Schilling, R. Willumeit, Effects of extracellular magnesium on the differentiation and function of human osteoclasts, Acta Biomater. 10 (2014) 2843–2854, https://doi.org/10.1016/j.actbio.2014.02.010.
[17] Y. Zhang, J. Xu, Y.C. Ruan, M.K. Yu, M. O'Laughlin, H. Wise, D. Chen, L. Tian, D. Shi, J. Wang, S. Chen, J.Q. Feng, D.H. Chow, X. Xie, L. Zheng, L. Huang, S. Huang, K. Leung, N. Lu, L. Zhao, H. Li, D. Zhao, X. Guo, K. Chan, F. Witte, H.C. Chan, Y. Zheng, L. Qin, Implant-derived magnesium induces local neuronal production of CGRP to improve bone-fracture healing in rats, Nat. Med. 22 (2016) 1160–1169, https://doi.org/10.1038/nm.4162.
[18] L. Zhang, J. Pei, H. Wang, Y. Shi, J. Niu, F. Yuan, H. Huang, H. Zhang, G. Yuan, Facile preparation of poly(lactic acid)/Brushite bilayer coating on biodegradable magnesium alloys with multiple functionalities for orthopedic application, ACS Appl. Mater. Interfaces 9 (2017) 9437–9448, https://doi.org/10.1021/acsami.7b00209.
[19] M. Ribeiro, F.J. Monteiro, M.P. Ferraz, Infection of orthopedic implants with emphasis on bacterial adhesion process and techniques used in studying bacterial-material interactions, Biomatter 2 (2012) 176–194, https://doi.org/10.4161/biom.22905.
[20] Y. Shao, R.-C. Zeng, S.-Q. Li, L.-Y. Cui, Y.-H. Zou, S.-K. Guan, Y.-F. Zheng, Advance in antibacterial magnesium alloys and surface coatings on magnesium alloys: a review, Acta Metall. Sin. 33 (2020) 615–629, https://doi.org/10.1007/s40195-020-01044-w.
[21] D.A. Robinson, R.W. Griffith, D. Shechtman, R.B. Evans, M.G. Conzemius, In vitro antibacterial properties of magnesium metal against Escherichia coli, Pseudomonas aeruginosa and Staphylococcus aureus, Acta Biomater. 6 (2010) 1869–1877, https://doi.org/10.1016/j.actbio.2009.10.007.
[22] N. Ahmad, N. Saad, Effects of antibiotics on dental implants: a review, J. Clin. Med. Res. 4 (2012) 1–6, https://doi.org/10.4021/jocmr658w.
[23] J.A. Cowan, Structural and catalytic chemistry of magnesium-dependent enzymes, Biometals 15 (2002) 225–235, https://doi.org/10.1023/A:1016022730880.
[24] K.A. Feeney, L.L. Hansen, M. Putker, C. Olivares-Yañez, J. Day, L.J. Eades, L.F. Larrondo, N.P. Hoyle, J.S. O'Neill, G. van Ooijen, Daily magnesium fluxes regulate cellular timekeeping and energy balance, Nature 532 (2016) 375, https://doi.org/10.1038/nature17407.
[25] A. Sargenti, G. Farruggia, N. Zaccheroni, C. Marraccini, M. Sgarzi, C. Cappadone, E. Malucelli, A. Procopio, L. Prodi, M. Lombardo, S. Iotti, Synthesis of a highly Mg^{2+}-selective fluorescent probe and its application to quantifying and imaging total intracellular magnesium, Nat. Protoc. 12 (2017) 461 https://doi.org/10.1038/nprot.2016.183 https://www.nature.com/articles/nprot.2016.183#supplementary-information.
[26] K. Nandakumar, K.R. Sreekumari, Y. Kikuchi, Antibacterial properties of magnesium alloy AZ31B: in - vitro studies using the biofilm-forming bacterium Pseudomonas sp, Biofouling 18 (2002) 129–135, https://doi.org/10.1080/08927010290032386.
[27] X. Zhu, Y. Liu, Q. Wang, J. Liu, Influence of sulfate-reducing bacteria on the corrosion residual strength of an AZ91D magnesium alloy, Materials 7 (2014) 7118–7129, https://doi.org/10.3390/ma7107118.
[28] H.-C. Flemming, J. Wingender, The biofilm matrix, Nat. Rev. Microbiol. 8 (2010) 623–633, https://doi.org/10.1038/nrmicro2415.
[29] W. Yan, Y.-J. Lian, Z.-Y. Zhang, M.-Q. Zeng, Z.-Q. Zhang, Z.-Z. Yin, L.-Y. Cui, R.-C. Zeng, In vitro degradation of pure magnesium—the synergetic influences of glucose and albumin, Bioact. Mater. 5 (2020) 318–333, https://doi.org/10.1016/j.bioactmat.2020.02.015.
[30] S.M. Marino, V.N. Gladyshev, Cysteine function governs its conservation and degeneration and restricts its utilization on protein surfaces, J. Mol. Biol. 404 (2010) 902–916, https://doi.org/10.1016/j.jmb.2010.09.027.
[31] C. Juillan-Binard, A. Picciocchi, J.P. Andrieu, J. Dupuy, I. Petit-Hartlein, C. Caux-Thang, C. Vives, V. Niviere, F. Fieschi, A two-component NADPH oxidase (NOX)-like system in bacteria is involved in the electron transfer chain to the methionine sulfoxide reductase MsrP, J. Biol. Chem. 292 (2017) 2485–2494, https://doi.org/10.1074/jbc.M116.752014.
[32] R.-C. Zeng, W. Dietzel, R. Zettler, W.-m. Gan, X.-x. Sun, Microstructural evolution and delayed hydride cracking of FSW-AZ31 magnesium alloy during SSRT, Trans. Nonferrous Metals Soc. China 24 (2014) 3060–3069, https://doi.org/10.1016/S1003-6326(14)63443-9.
[33] Rong-Chang Zeng, Zheng-Zheng Yin, Xiao-Bo Chen, Dao-Kui Xu, Corrosion types of magnesium alloys, in: W.B.a.M.K. Tomasz Tański (Ed.), Corrosion Types of Magnesium Alloys, Magnesium Alloys - Selected Issue, IntechOpen, 2018.
[34] Y. Liu, X. Liu, Z. Zhang, N. Farrell, D. Chen, Y. Zheng, Comparative, real-time in situ monitoring of galvanic corrosion in Mg-Mg_2Ca and Mg-$MgZn_2$ couples in Hank's solution, Corrosion Sci. 161 (2019) 108185, https://doi.org/10.1016/j.corsci.2019.108185.
[35] Y. Yao, S. Zhu, H. Wang, H. Li, M. Shao, A spectroscopic study on the nitrogen electrochemical reduction reaction on gold and platinum surfaces, J. Am. Chem. Soc. 140 (2018) 1496–1501, https://doi.org/10.1021/jacs.7b12101.
[36] A. Alvarez-Ordóñez, D.J.M. Mouwen, M. López, M. Prieto, Fourier transform infrared spectroscopy as a tool to characterize molecular composition and stress response in foodborne pathogenic bacteria, J. Microbiol. Methods 84 (2011) 369–378, https://doi.org/10.1016/j.mimet.2011.01.009.
[37] Z. Movasaghi, S. Rehman, D.I. ur Rehman, Fourier transform infrared (FTIR) spectroscopy of biological tissues, Appl. Spectrosc. Rev. 43 (2008) 134–179, https://doi.org/10.1080/05704920701829043.
[38] J. Depciuch, A. Stanek-Widera, M. Warchulska, D. Lange, K. Sarwa, A. Koziorowska, M. Kula, J. Cebulski, Identification of chemical changes in healthy breast tissue caused by chemotherapy using Raman and FTIR spectroscopy: a preliminary study, Infrared Phys. Technol. 102 (2019) 102989, https://doi.org/10.1016/j.infrared.2019.102989.
[39] Y. Wang, L.Y. Cui, R.-C. Zeng, S.Q. Li, Y.H. Zou, E.H. Han, In vitro degradation of PureMagnesium-the effects of glucose and/or amino acid, Materials 10 (2017) 16, https://doi.org/10.3390/ma10070725.
[40] P.F. Beese-Vasbender, S. Nayak, A. Erbe, M. Stratmann, K.J.J. Mayrhofer, Electrochemical characterization of direct electron uptake in electrical microbially influenced corrosion of iron by the lithoautotrophic SRB Desulfopila corrodens strain IS4, Electrochim. Acta 167 (2015) 321–329, https://doi.org/10.1016/j.electacta.2015.03.184.
[41] Y. Yang, A.J. Wikieł, L.T. Dall'Agnol, P. Eloy, M.J. Genet, J.J.G. Moura, W. Sand, C.C. Dupont-Gillain, P.G. Rouxhet, Proteins dominate in the surface layers formed on materials exposed to extracellular polymeric substances from bacterial cultures, Biofouling 32 (2016) 95–108, https://doi.org/10.1080/08927014.2015.1114609.
[42] L.Y. Li, L.Y. Cui, B. Liu, R.-C. Zeng, X.B. Chen, S.Q. Li, Z.L. Wang, E.H. Han, Corrosion resistance of glucose-induced hydrothermal calcium phosphate coating on pure magnesium, Appl. Surf. Sci. 465 (2019) 1066–1077, https://doi.org/10.1016/j.apsusc.2018.09.203.
[43] J. Jin, G. Wu, Z. Zhang, Y. Guan, Effect of extracellular polymeric substances on corrosion of cast iron in the reclaimed wastewater, Bioresour. Technol. 165 (2014) 162–165, https://doi.org/10.1016/j.biortech.2014.01.117.
[44] R.R. Mawlankar, P. Mual, V.V. Sonalkar, M.N. Thorat, A. Verma, K. Srinivasan,

S.G. Dastager, Microbacterium enclense sp. nov., isolated from sediment sample, Int. J. Syst. Evol. Microbiol. 65 (2015) 2064–2070, https://doi.org/10.1099/ijs.0.000221.
[45] Y.J. Kim, S.W. Roh, M.J. Jung, M.S. Kim, E.J. Park, J.W. Bae, Microbacterium mitrae sp. nov., isolated from salted turban shell, Int. J. Syst. Evol. Microbiol. 61 (2011) 399–403, https://doi.org/10.1099/ijs.0.021519-0.
[46] C.T. Gu, C.Y. Li, L.J. Yang, G.C. Huo, Enterobacter xiangfangensis sp. nov., isolated from Chinese traditional sourdough, and reclassification of Enterobacter sacchari Zhu et al. 2013 as Kosakonia sacchari comb. nov, Int. J. Syst. Evol. Microbiol. 64 (2014) 2650–2656, https://doi.org/10.1099/ijs.0.064709-0.
[47] J. Gao, K. Xu, H. Liu, G. Liu, M. Bai, C. Peng, T. Li, Y. Yin, Impact of the gut microbiota on intestinal immunity mediated by tryptophan metabolism, Front. Cell. Infect. Microbiol 8 (2018) 13, https://doi.org/10.3389/fcimb.2018.00013.
[48] S.S. Maktedar, S.S. Mehetre, G. Avashthi, M. Singh, In situ sonochemical reduction and direct functionalization of graphene oxide: a robust approach with thermal and biomedical applications, Ultrason. Sonochem. 34 (2017) 67–77, https://doi.org/10.1016/j.ultsonch.2016.05.015.
[49] W. Yan, Y. Xiao, W. Yan, R. Ding, S. Wang, F. Zhao, The effect of bioelectrochemical systems on antibiotics removal and antibiotic resistance genes: a review, Chem. Eng. J. 358 (2019) 1421–1437, https://doi.org/10.1016/j.cej.2018.10.128.
[50] L. Grenho, M.C. Manso, F.J. Monteiro, M.P. Ferraz, Adhesion of Staphylococcus aureus, Staphylococcus epidermidis, and Pseudomonas aeruginosa onto nanohydroxyapatite as a bone regeneration material, J. Biomed. Mater. Res. 100A (2012) 1823–1830, https://doi.org/10.1002/jbm.a.34139.
[51] D.T. Huang, D.M. Yealy, M.R. Filbin, A.M. Brown, C.C.H. Chang, Y. Doi, M.W. Donnino, J. Fine, M.J. Fine, M.A. Fischer, J.M. Holst, P.C. Hou, J.A. Kellum, F. Khan, M.C. Kurz, S. Lotfipour, F. LoVecchio, O. Peck-Palmer, F. Pike, H. Prunty, R.L. Sherwin, L. Southerland, T. Terndrup, L.A. Weissfeld, J. Yabes, D.C. Angus, A.C.T.I. Pro, Procalcitonin-guided use of antibiotics for lower respiratory tract infection, N. Engl. J. Med. 379 (2018) 236–249, https://doi.org/10.1056/NEJMoa1802670.
[52] Y.J. Kim, S.W. Roh, M.J. Jung, M.S. Kim, E.J. Park, J.W. Bae, Microbacterium mitrae sp. nov., isolated from salted turban shell, Int. J. Syst. Evol. Microbiol. 61 (2011) 399–403, https://doi.org/10.1099/ijs.0.021519-0.
[53] C.T. Gu, C.Y. Li, L.J. Yang, G.C. Huo, Enterobacter xiangfangensis sp. nov., isolated from Chinese traditional sourdough, and reclassification of Enterobacter sacchari Zhu et al. 2013 as Kosakonia sacchari comb. nov, Int. J. Syst. Evol. Microbiol. 64 (2014) 2650–2656, https://doi.org/10.1099/ijs.0.064709-0.
[54] M. Ascencio, M. Pekguleryuz, S. Omanovic, An investigation of the corrosion mechanisms of WE43 Mg alloy in a modified simulated body fluid solution: the effect of electrolyte renewal, Corrosion Sci. 91 (2015) 297–310, https://doi.org/10.1016/j.corsci.2014.11.034.
[55] D. Davies, Understanding biofilm resistance to antibacterial agents, Nat. Rev. Drug Discov. 2 (2003) 114–122, https://doi.org/10.1038/nrd1008.
[56] P. Baker, P.J. Hill, B.D. Snarr, N. Alnabelseya, M.J. Pestrak, M.J. Lee, L.K. Jennings, J. Tam, R.A. Melnyk, M.R. Parsek, D.C. Sheppard, D.J. Wozniak, P.L. Howell, Exopolysaccharide biosynthetic glycoside hydrolases can be utilized to disrupt and prevent Pseudomonas aeruginosa biofilms, Sci Adv 2 (2016), https://doi.org/10.1126/sciadv.1501632 e1501632-e1501632.
[57] N.T. Kirkland, N. Birbilis, M.P. Staiger, Assessing the corrosion of biodegradable magnesium implants: a critical review of current methodologies and their limitations, Acta Biomater. 8 (2012) 925–936, https://doi.org/10.1016/j.actbio.2011.11.014.